Electronic Supplementary Information for

Switchover from Singlet Oxygen to Superoxide Radical through a Photoinduced Two-Step Sequential Energy Transfer Process

Shengsheng Yu,[‡a] Rong-Xin Zhu,[‡a] Kai-Kai Niu,[a] Ning Han,[b] Hui Liu,[a] and Ling-Bao Xing*[a]

[a]School of Chemistry and Chemical Engineering, Shandong University of Technology, Zibo, Shandong 255000, P. R. China

[b]Department of Materials Engineering, KU Leuven, Leuven 3001, Belgium

E-mail: lbxing@sdut.edu.cn

[‡]These authors contributed equally to this work.

Experimental

Materials: Unless specifically mentioned, all chemicals are commercially available and were used as received.

Characterizations

^{1}H NMR spectra were recorded on a Bruker Avance 400 spectrometer (400 MHz) at 298 K, and the chemical shifts (δ) were expressed in ppm, and *J* values were given in Hz. UV-vis spectra were obtained on a Shimadzu UV-1601PC spectrophotometer in a quartz cell (light path 10 mm) at 298 K. Steady-state fluorescence measurements were carried out using a Hitachi 4500 spectrophotometer. Dynamic light scattering (DLS) and zeta potential are measured on Malvern Zetasizer Nano ZS90. Transmission electron microscopy (TEM) images were obtained on a JEM 2100 operating at 120 kV. Samples for TEM measurement was prepared by dropping the mixed aqueous solution on a carbon-coated copper grid (300 mesh) and drying by slow evaporation. Hamamatsu absolute quantum yield measuring instrument Quantaurus-QY was used to obtain fluorescence quantum yields. The time-resolved fluorescence decay curve was obtained by the FLS 920 Steady-State/Transient Fluorescence Spectrometer.

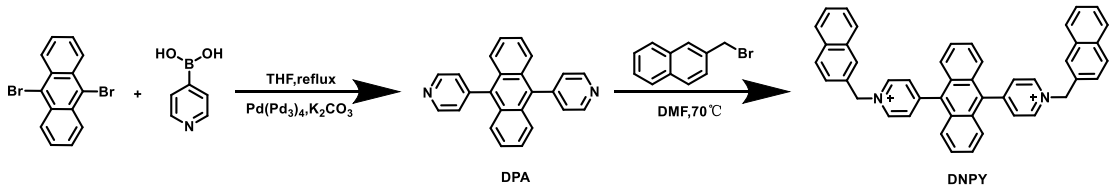

Scheme S1. Synthetic route of DNPY.

Synthesis of DPA

9,10-dibromoanthracene (2.07 g, 6 mmol), 4-pyridinyl boronic acid (2.21 g, 18 mmol), tetrakis(triphenylphosphine)palladium (0.14 g, 0.12 mmol) were added into the mixed solution of tetrahydrofuran (15 mL), toluene (3 mL) and 6 mL of 2 mol/L aqueous potassium carbonate. The mixture was refluxed under nitrogen for 3 days, filtered, and the precipitate was collected and washed with H_2O and methanol. ^{1}H NMR (400 MHz, DMSO-d_6) δ 8.89 (d, J = 5.9 Hz, 4H), 7.57 - 7.53 (m, 8H), 7.51 (d, J = 10.3 Hz, 4H).

Energy-transfer efficiency calculation

The energy-transfer efficiency (Φ_{ET}) was calculated from excitation fluorescence spectra through the equation S1:

$$\Phi_{ET} = 1\text{-}I_{DA}/I_D \quad (S1)$$

Where I_{DA} and I_D are the fluorescence intensities of the emission of DNPY-SBE-β-CD+RhB, DNPY-SBE-β-CD+RhB+SR101, or DNPY-SBE-β-CD+SR101 (donor and acceptor) and DNPY-SBE-β-CD or DNPY-SBE-β-CD+RhB (donor) respectively, when excited at 409 nm. The energy-transfer efficiency (Φ_{ET}) was calculated as 76%, 81% and 84% in an aqueous environment, measured under the condition of [DNPY] = 1.0×10^{-5} mol/L, [SBE-β-CD] = 2.0×10^{-6} mol/L, [RhB] = 1.0×10^{-6} mol/L, [SR101] = 1.0×10^{-6} mol/L.

Antenna effect calculation

The Antenna effect was calculated based on the excitation spectra using equation S2:

$$\text{Antenna effect} = (I_{DA,409} - I_{D,409}) / I_{DA,550/580} \quad (S2)$$

Where I_{DA} and I_D are the fluorescence intensities of the emission of DNPY-SBE-β-CD+RhB, DNPY-SBE-β-CD+RhB+SR101, or DNPY-SBE-β-CD+SR101 (donor and acceptor) and DNPY-SBE-β-CD or DNPY-SBE-β-CD+RhB (donor) respectively, when excited at 409 nm. The antenna effect value was calculated as 15.7, 7.4 and 7.5 in water, measured under the condition of [DNPY] = 1.0×10^{-5} mol/L, [SBE-β-CD] = 2.0×10^{-6} mol/L, [RhB] = 1.0×10^{-6} mol/L, [SR101] = 1.0×10^{-6} mol/L.

Procedure for $^1O_2$ Quantum Yield Measurement.

The $^1O_2$ quantum yield was measured using Rose Bengal (RB) as the reference photosensitizer and calculated using the following S3:

$$\Phi_{probe}=\Phi_{RB}\times(K_{probe}A_{RB}/\ K_{RB}A_{probe})\ (S3)$$

where Kprobe and K_{RB} are the decomposition rate constants of ABDA in the presence of the probe and RB, respectively. Φ_{RB} is the $^1O_2$ quantum yield of RB (Φ_{RB} = 0.75 in water). A_{probe} and A_{RB} represent the integration area of absorption bands ranging from 410 to 415 nm of the probe and RB, respectively. The ABDA (1.5×10^{-7} mol) in 3 mL of the probe solution was exposed to purple light irradiation (410-415 nm) with a power density of 10W. The natural logarithm of the absorbance ratio (A_0/A) of ABDA at 380 nm was plotted against irradiation time and the slope is regarded as the decomposition rate.

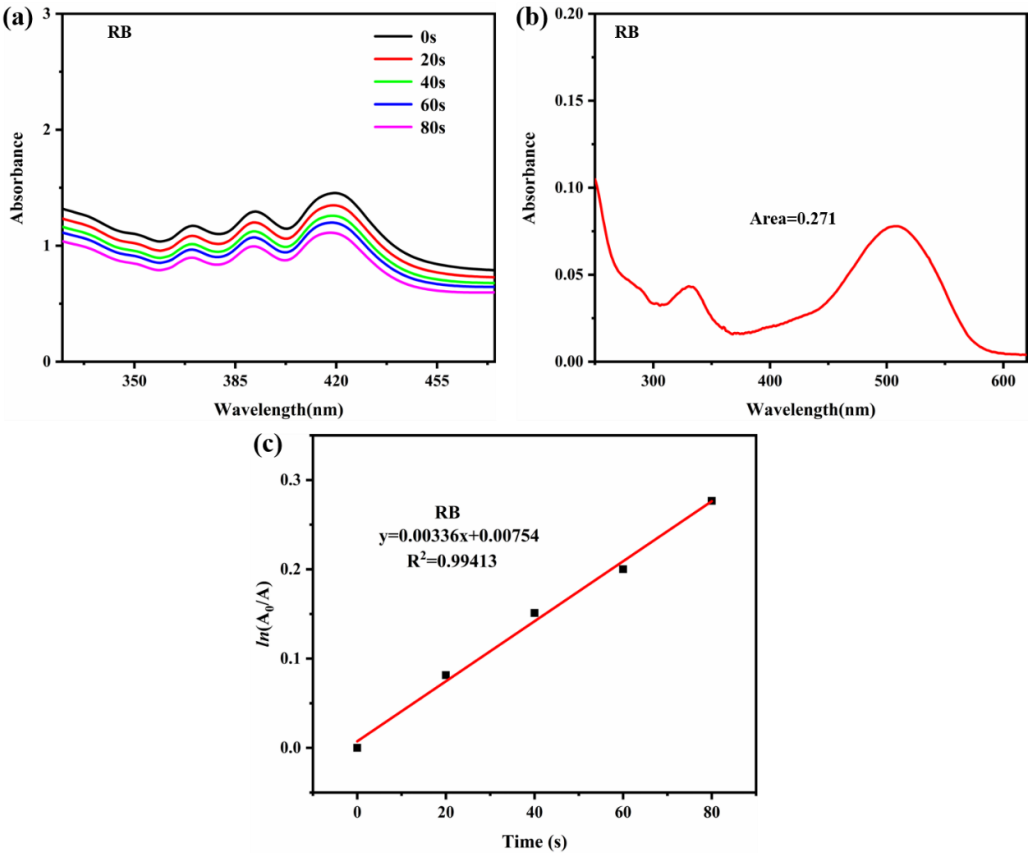

Fig. S1 (a) The absorption spectra of ABDA after irradiation (410-415 nm, 10 W) for different time in the presence of RB; (b) The UV-vis absorption spectra of RB in the aqueous solution; (c) The decomposition rates of ABDA in the presence of RB.

Procedure for $O_2^{\bullet-}$ Generation Efficiency Measurement.

The amounts of $O_2^{\bullet-}$ was quantitatively detected by nitroblue tetrazolium (NBT) conversion detection. NBT, which can react with $O_2^{\bullet-}$ and displays a maximum absorbance at 260 nm, was selected to determine the amounts of $O_2^{\bullet-}$ generated over the photocatalysts. By recording the concentration of NBT on a UV-vis spectrophotometer, the production of $O_2^{\bullet-}$ was quantitatively analyzed. First, the photocatalyst (3.0×10^{-8} mol) and NBT (9.0×10^{-8} mol) sonication were dispersed into 3 mL of aqueous solution. Then, the mixture was exposed to 410-415nm LED (10W). At appropriate intervals, record the change in absorbance of NBT at 260 nm by UV-vis spectrophotometer, the production of $O_2^{\bullet-}$ was quantitatively analyzed.

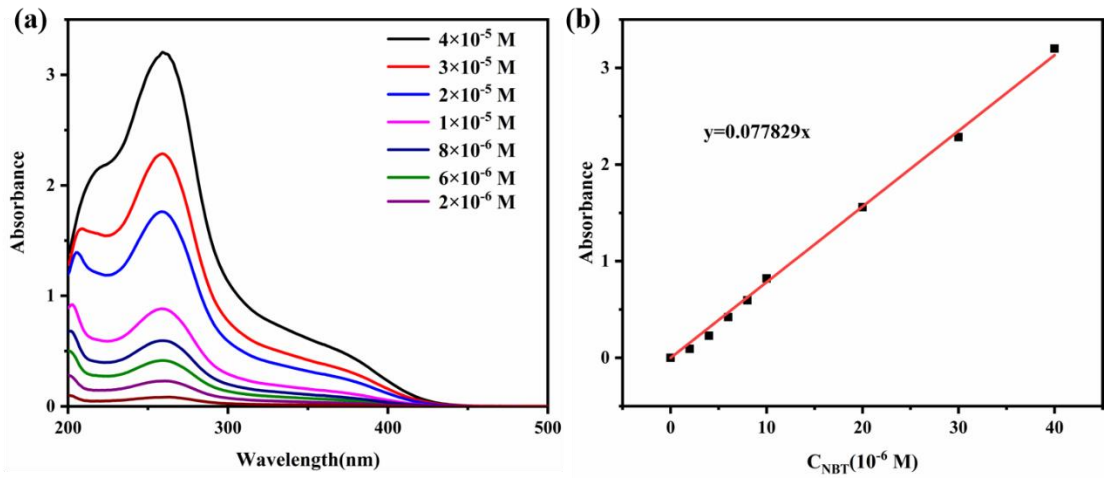

Fig. S2 (a) The UV-vis absorption spectra of different concentrations of NBT in the aqueous solution; (b) the relation curve of UV-vis absorption intensity of NBT at 260 nm and NBT concentration in aqueous solutions.

General procedure for the photooxidation reaction of thioanisole and its derivatives

The thioanisole or its derivatives (0.10 mmol) was dissolved in freshly prepared aqueous solution (catalyst total amount: 3 mL**,** [DNPY] = 1.67×10^{-4} mol/L, [SBE-β-CD] = 3.33×10^{-5} mol/L). The mixture was irradiated with 410-415 nm LED (10 W) at room temperature for 2 h. Then,

the mixture was extracted with dichloromethane and dried with anhydrous Na_2SO_4. Then the organic solution was concentrated in a vacuum and purified by rapid column chromatography to obtain the corresponding products.

General procedure for the photocatalytic oxidative hydroxylation of arylboronic acids

The arylboronic acids (0.10 mmol), *N,N*-diisopropylethylamine (DIPEA) (70 μL, 0.40 mmol) were dissolved freshly prepared aqueous solution (catalyst total amount: 3 mL**,** [DNPY] = 1.67×10^{-4} mol/L, [SBE-β-CD] = 3.33×10^{-5} mol/L, [RhB] = 1.67×10^{-5} mol/L, [SR101] = 1.67×10^{-5} mol/L. The mixture was irradiated with 410-415 nm LED (10 W) at room temperature for 12 h. Then, the mixture was extracted with dichloromethane and dried with anhydrous Na_2SO_4. Then the organic solution was concentrated in a vacuum and purified by rapid column chromatography to obtain the corresponding products.

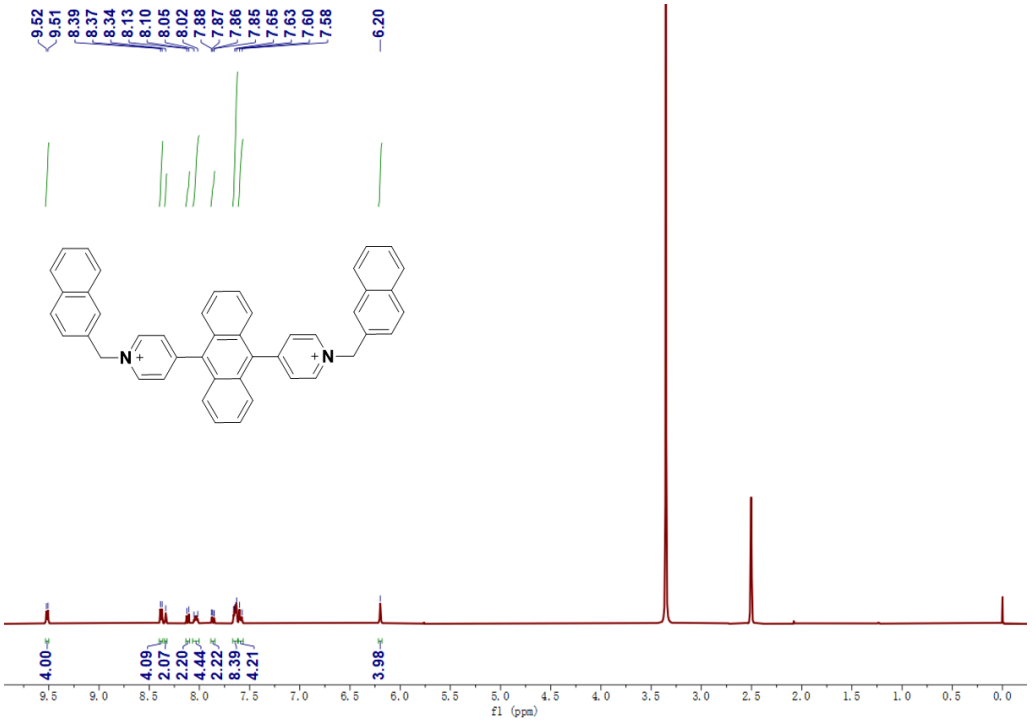

Fig. S3 ^{1}H NMR spectra of **DNPY** in DMSO-d_6.

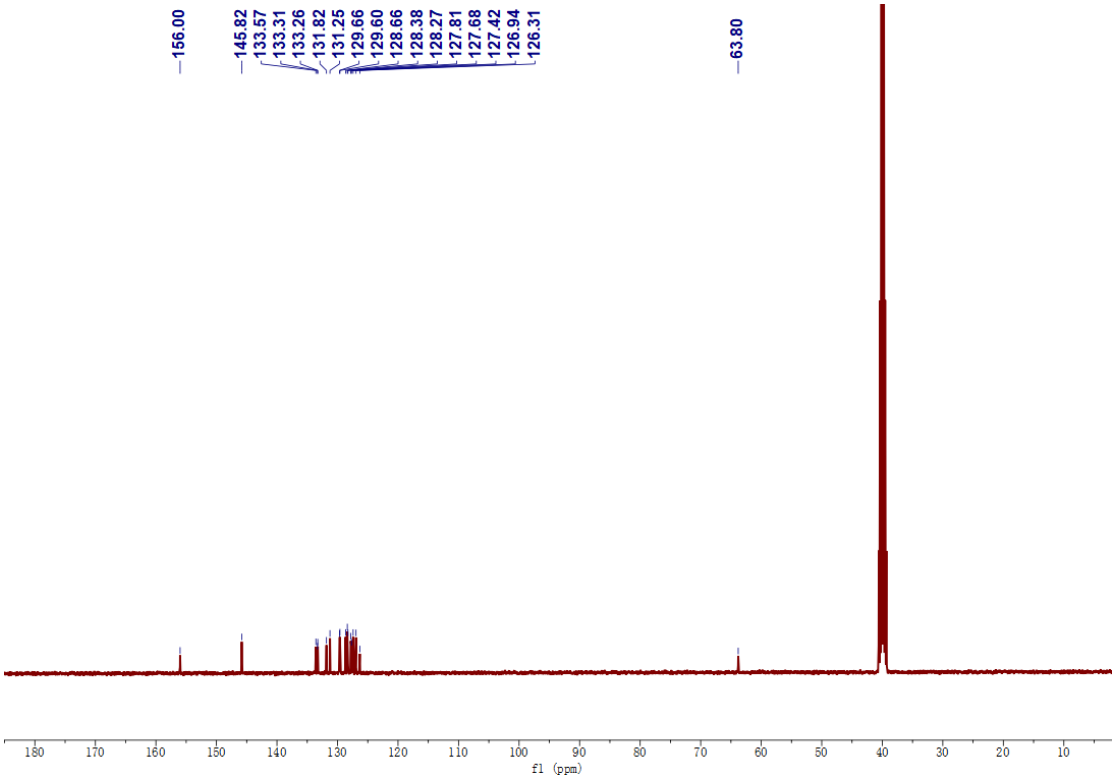

Fig. S4 ^{13}C NMR spectra of **DNPY** in DMSO-d_6.

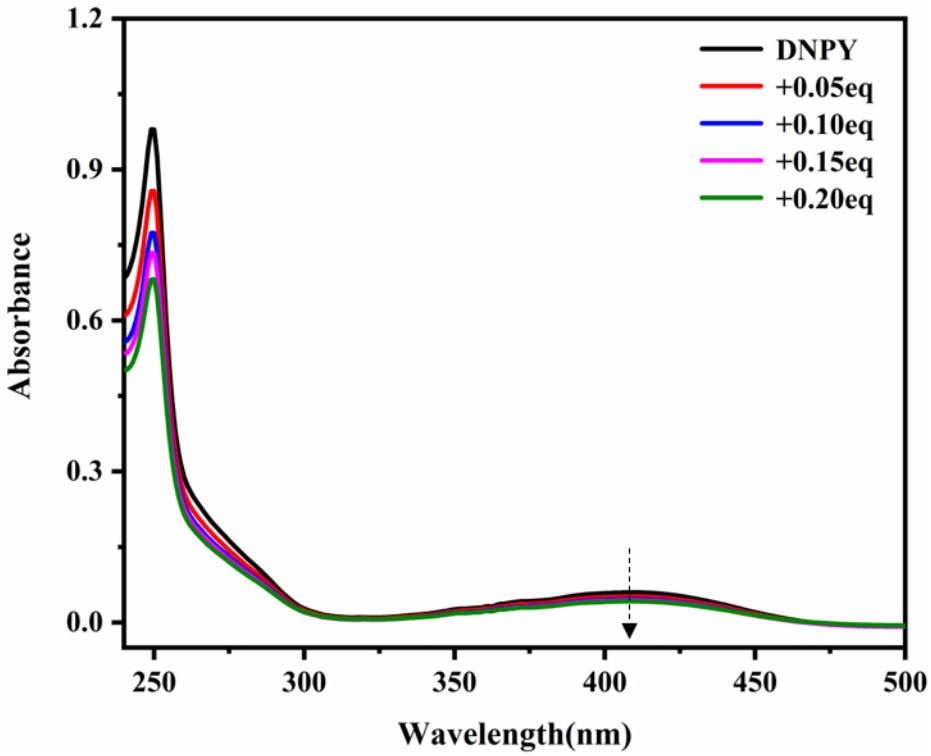

Fig. S5 The UV-vis absorption spectra of DNPY with gradual addition of SBE-β-CD in the aqueous solution. [DNPY] = 1.0×10^{-5} mol/L.

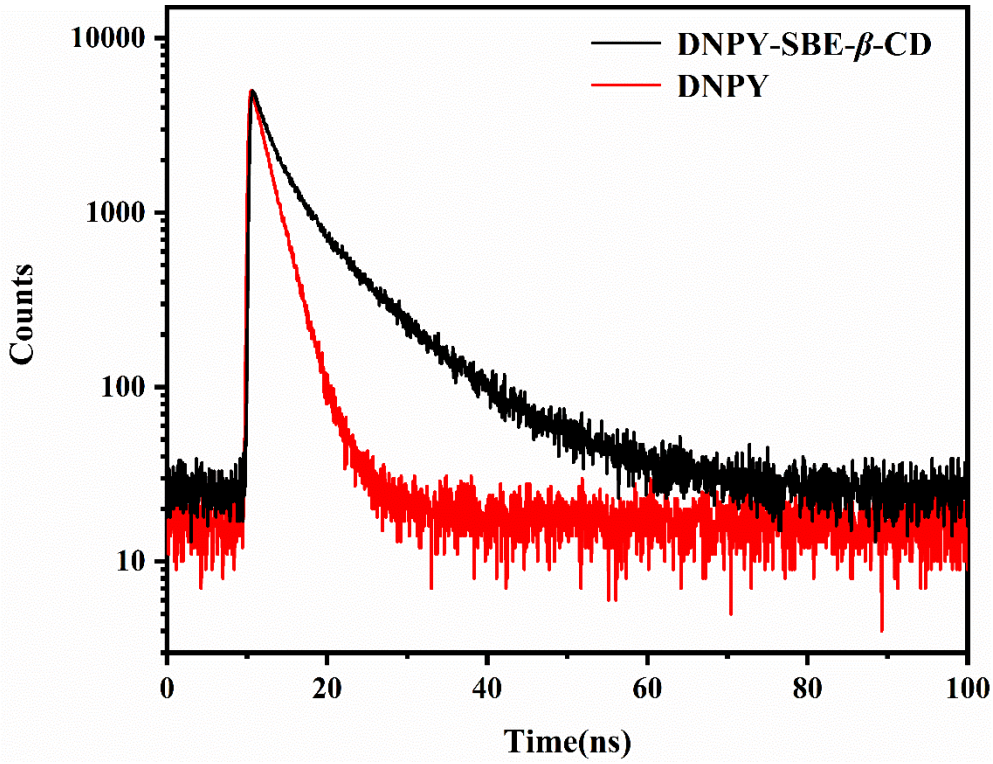

Fig. S6 Time-resolved fluorescence decay curves of DNPY and DNPY-SBE-β-CD. [DNPY] = 1.0 × 10^{-5} mol/L, [SBE-β-CD] = 2.0 × 10^{-6} mol/L.

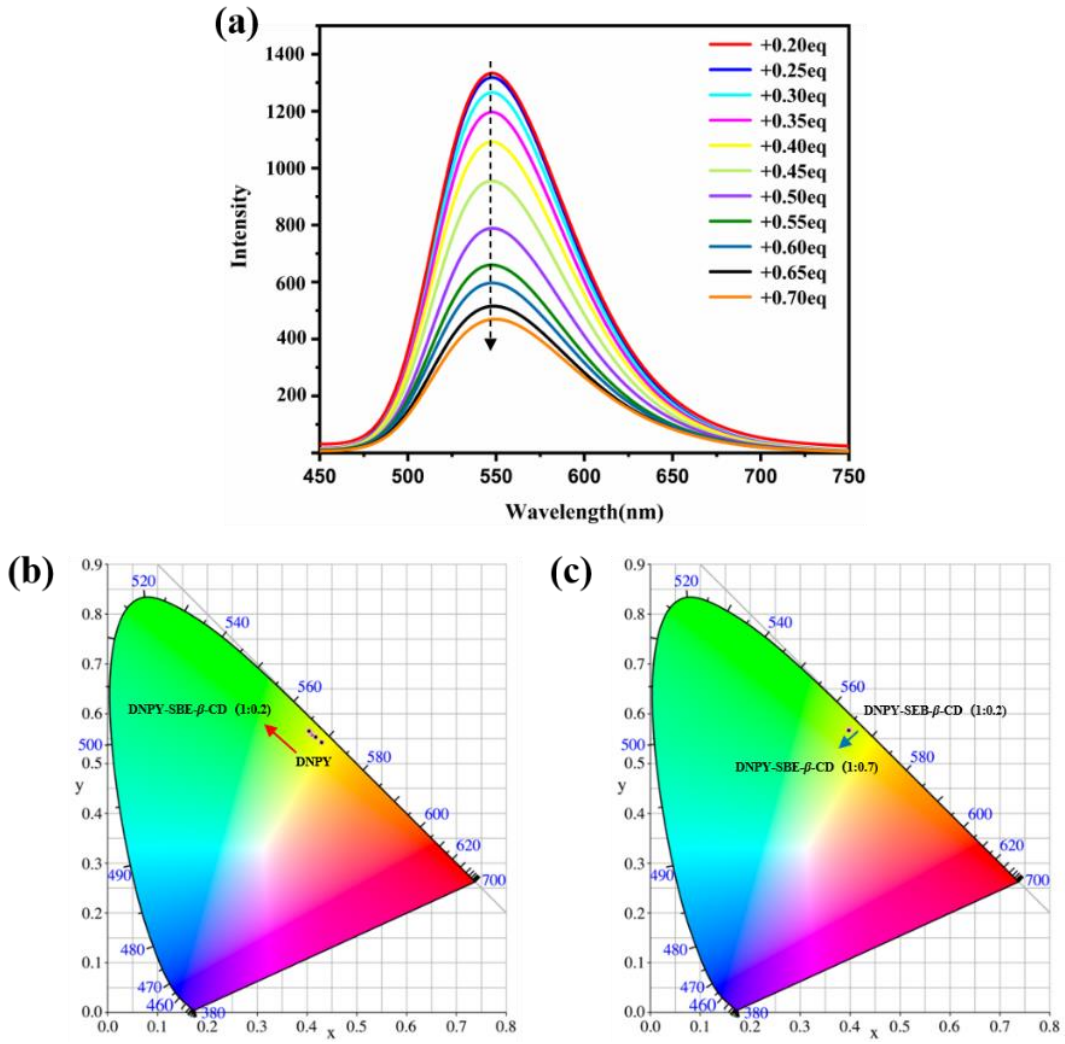

Fig. S7 (a) Fluorescence emission spectra of DNPY in aqueous solutions with different concentrations of SBE-β-CD (from 0.20 equiv. to 0.70 equiv.); (b) CIE chromaticity coordinates of DNPY at different concentrations of SBE-β-CD (from 0 to 0.20 equiv.); (c) CIE chromaticity coordinates of DNPY at different concentrations of SBE-β-CD (from 0.20 equiv. to 0.70 equiv.). [DNPY] = 1.0×10^{-5} mol/L, [SBE-β-CD] = 2.0×10^{-6} mol/L.

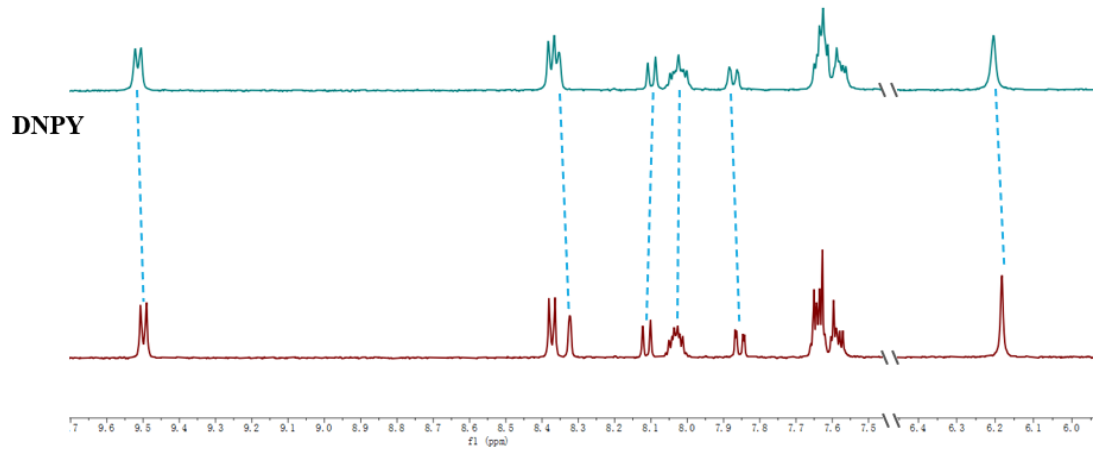

Fig. S8 ^{1}H NMR spectra of DNPY in the presence of 0.20 equiv. SBE-β-CD in DMSO-d_6. [DNPY] = 1.0×10^{-5} mol/L, [SBE-β-CD] = 2.0×10^{-6} mol/L.

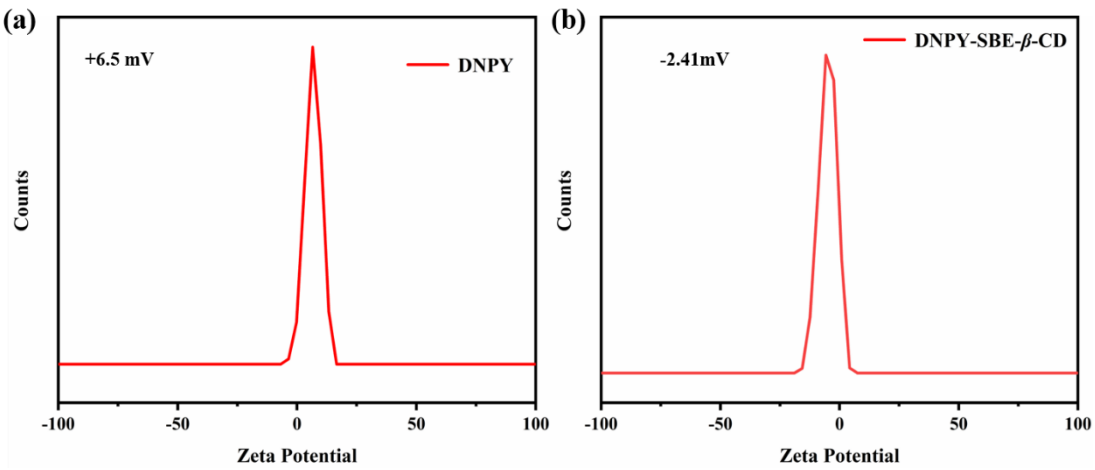

Fig. S9 Zeta potential of DNPY before and after the addition of 0.20 equiv. SBE-β-CD. [DNPY] = 1.0×10^{-5} mol/L, [SBE-β-CD] = 2.0×10^{-6} mol/L.

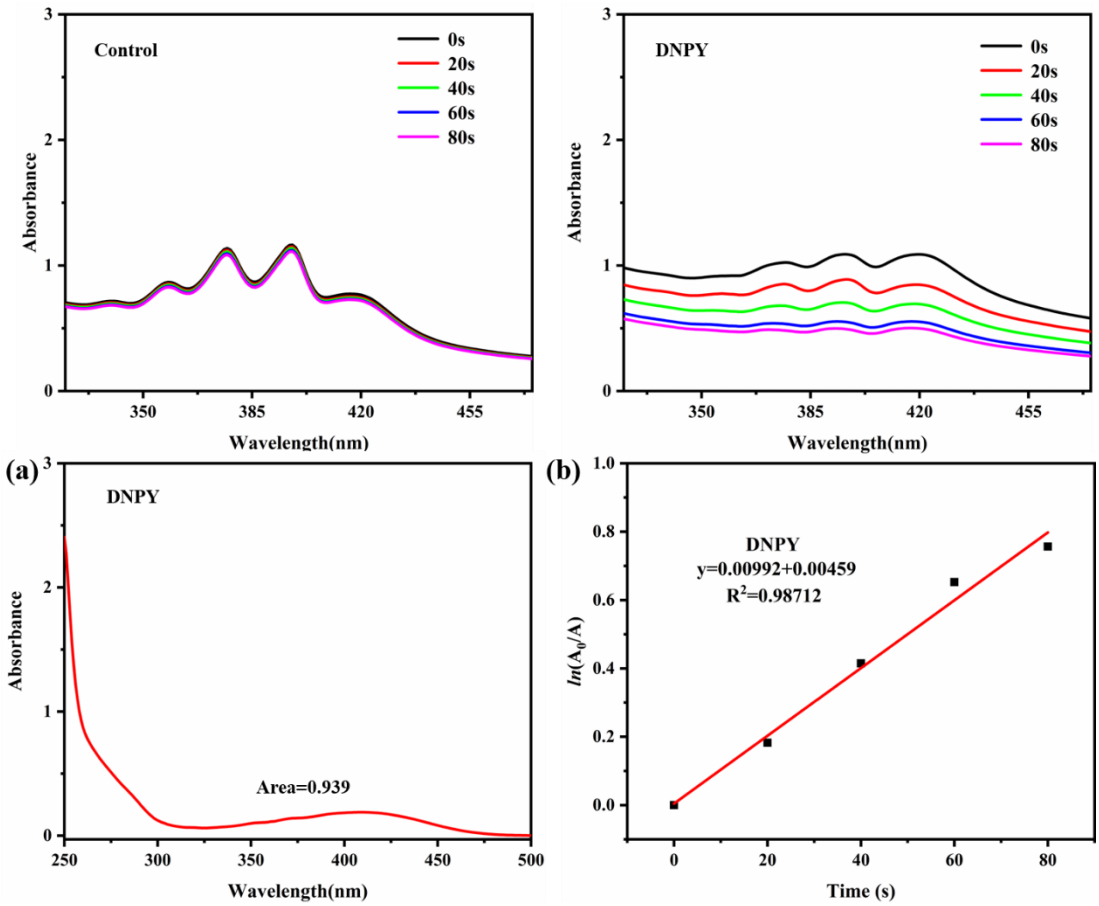

Fig. S10 The absorption spectra of ABDA after irradiation (410-415 nm, 10 W) for different time in the presence of (a) Control: ABDA without any additive; (b) DNPY; (c) The UV-vis absorption spectra of DNPY in the aqueous solution; (d) The decomposition rates of ABDA in the presence of DNPY.

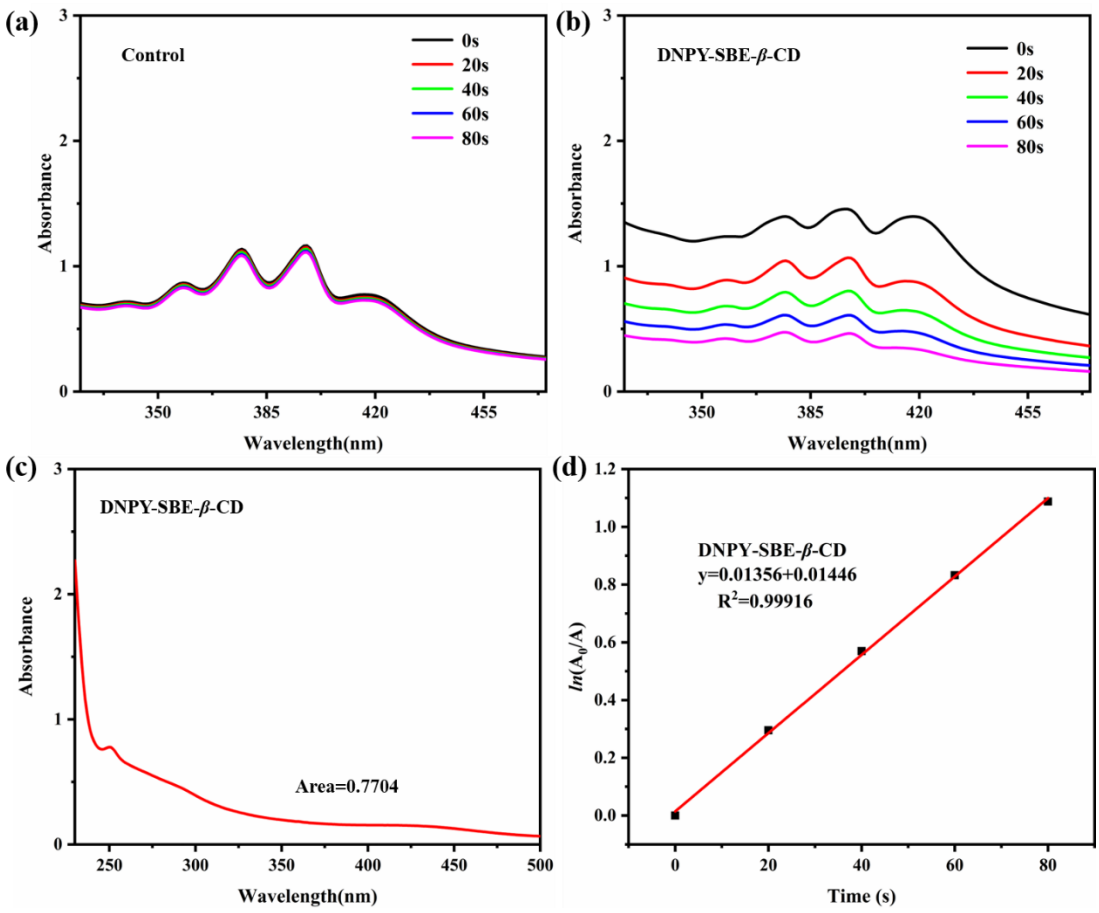

Fig. S11 The absorption spectra of ABDA after irradiation (410-415 nm, 10 W) for different time in the presence of (a) Control: ABDA without any additive; (b) DNPY-SBE-β-CD; (c) The UV-vis absorption spectra of DNPY-SBE-β-CD in the aqueous solution; (d) The decomposition rates of ABDA in the presence of DNPY-SBE-β-CD.

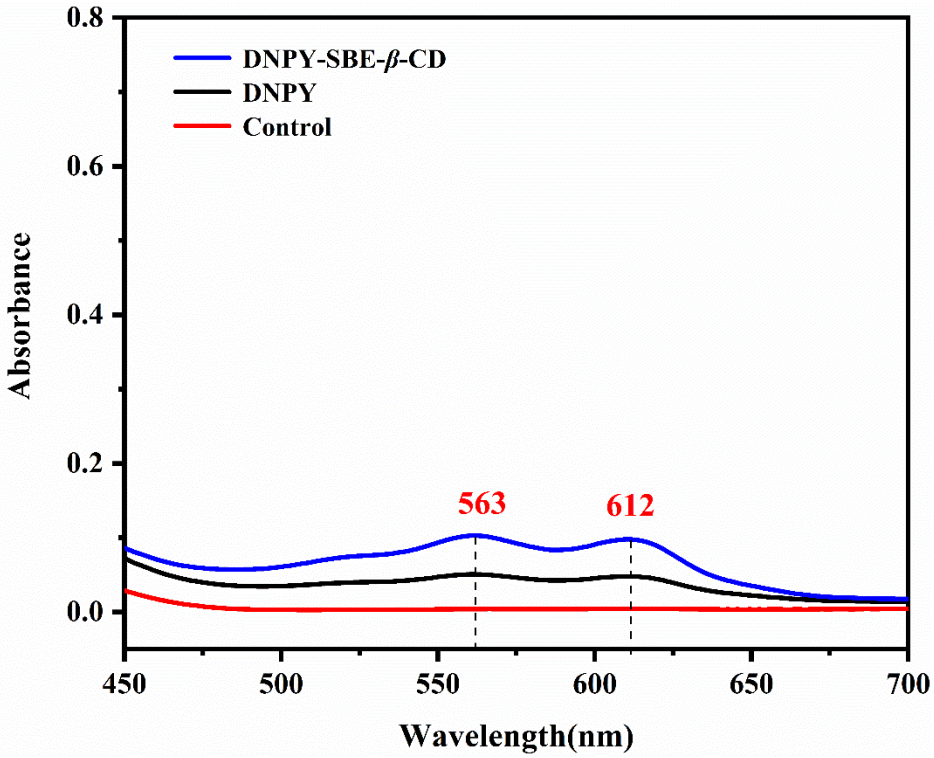

Fig. S12 UV-vis absorption spectra for cationic radicals of TMPD generated by indicated samples under the same conditions (Control: TMPD without any additive).

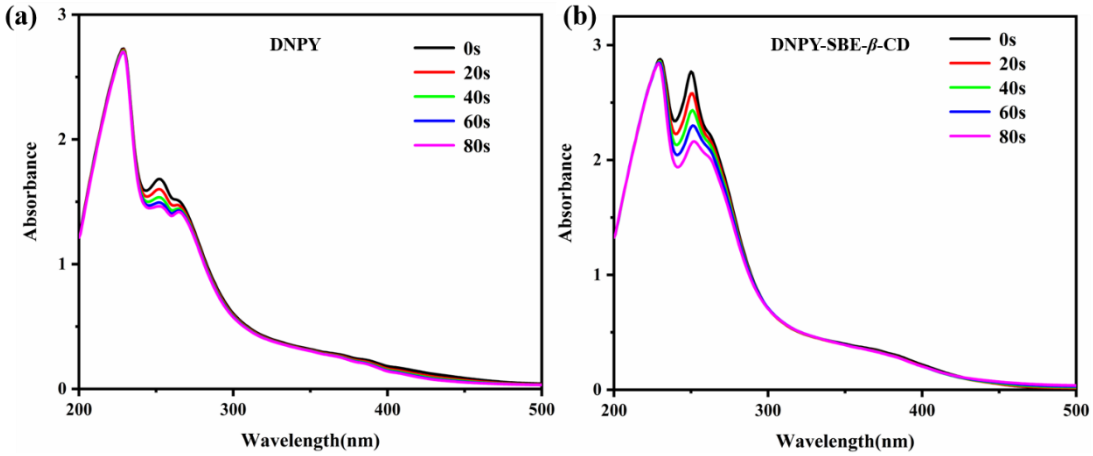

Fig. S13 The absorption spectra of NBT after irradiation (410-415 nm, 10 W) for different times in the presence of (a) DNPY; (b) DNPY-SBE-β-CD.

Table S1 Comparison of $^1O_2$ production efficiencies.

Entry	Systems	Φ_Δ ($^1O_2$)	literatures
1	NI-S	0.32	S1
2	MONI-S	0.74	
3	MANI-S	~1.00	
4	mCN-2I-BODIPY	0.526	S2
5	TPP	0.576	
6	mTz-2I-BODIPY	0.217	
7	pNH-Tz-2I-BODIPY	0.440	
8	pNH-Tz-TPP	0.591	
9	(mTz-Nor)-2I-BODIPY	0.505	
10	pNH-(Tz-Nor)-2I-BODIPY	0.473	
11	pNH-(Tz-Nor)-TPP	0.581	
12	P_2	0.14	S3
13	P_2-NMeI	0.50	
14	P_2C_2-NMeI	0.25	
15	P_2-NMeOAc	0.36	
16	P_2-SO_3NH_4	0.59	
17	P_2C_2-CO_2NH_4	0.24	
18	P_2-Suc	0.43	
19	H_2TCPP	0.53	S4
20	PCN-222/MOF545(FB)	0.35	
21	(R)-DTP-COF-QA	0.57	S5
22	TfR/TPETH-2T7	0.92	S6
23	TPCI	0.986	S7
24	1•4Cl^-	1.30	S8
25	1•2Cl^-	0.67	
26	TTDPzMg(H_2O)	0.30	S9
27	TTDPzGaCl	0.69	
28	TTDPzAlCl	0.35	
29	TTDPzCd	≤0.2	
30	TTDPzCu	0.08	
31	TTDPzZn	0.52	
32	3,4-TPyPzZn	0.56	S10
33	2,3-TPyPzZn	0.16	S11
34	TPyzPzZn	0.487	S12
35	ZnPc	0.56	S13
36	ZnPc 6	0.47	S14
37	1	0.23	S15
38	4	0.196	S16
39	[($PtCl_2$)LMg(H_2O)]	0.40	S17

40	16	0.137	S18
41	19	0.0073	S19
42	10	0.42	S20
43	[{Pd(OAc)2}4LZn]	0.43	S21
44	4b	0.54	S22
45	ZnTM2,3PyPz	0.65	S23
46	ZnPc 2	0.50	S24
47	$ZnAPc^{4+}$	0.50	S25
48	ZnPc 1	0.50	S26
49	3	0.72	S27
50	DNPY DNPY-SBE-β-CD DNPY-SBE-β-CD+RhB, DNPY-SBE-β-CD+SR101 DNPY-SBE-β-CD+RhB+SR101	0.597 0.994 0.069 0.042 0.054	This work

Table S2 Comparison of $O_2^{\bullet-}$ production efficiencies.

Entry	Systems	$\Phi_{\triangle}$ ($O_2^{\bullet-}$)	literatures
1	20%BI	67%（NBT）	S28
2	BiOBr	10.9%（NBT）	S29
3	TiO_2	8.0 μM	S30
4	CeO_2	8.4 μM	
5	SiO_2	-	
6	Al_2O_3	-	
7	ZnO	167 μM	
8	CuO	-	
9	Fe_2O_3	18.1 μM	
10	Disrupted NanoMANI-S	3.0-fold greater amount of $O_2^{\bullet-}$ than MB	S1
11	DNPY DNPY-SBE-β-CD DNPY-SBE-β-CD+RhB DNPY-SBE-β-CD+SR101 DNPY-SBE-β-CD+RhB+SR101	6.3% 9.2% 19.7% 24.9% 44.1%	This work

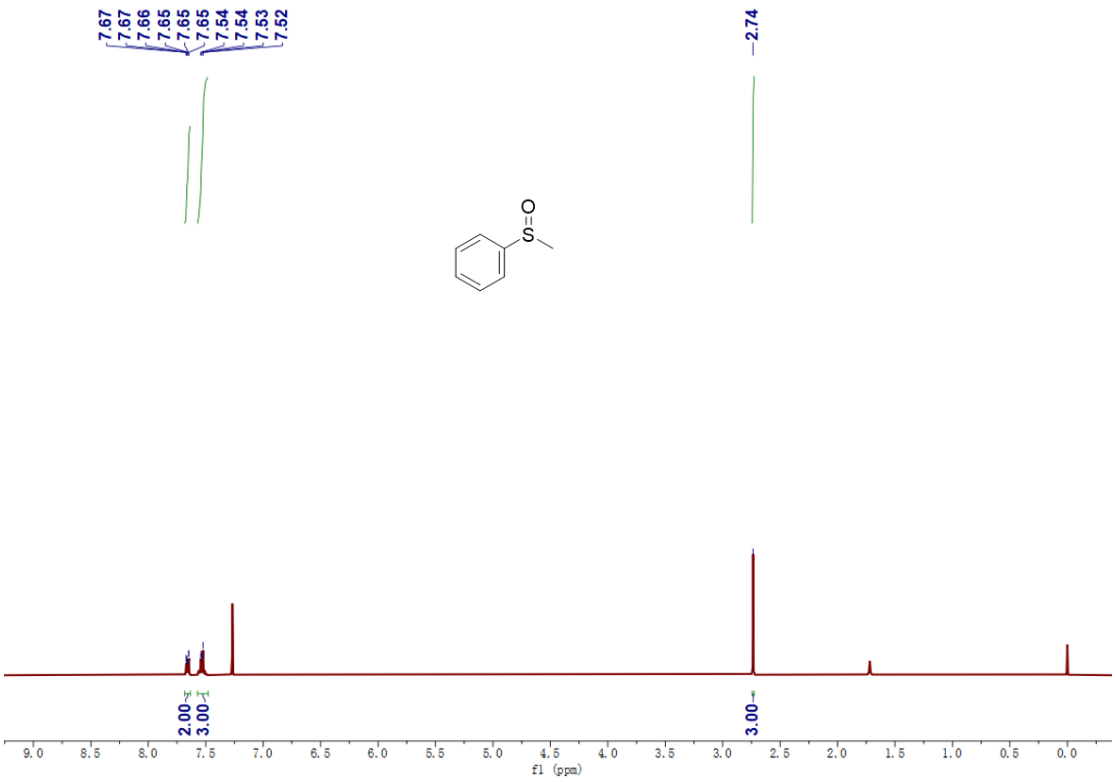

Fig. S14 ^{1}H NMR spectra of **2a** in $CDCl_3$.

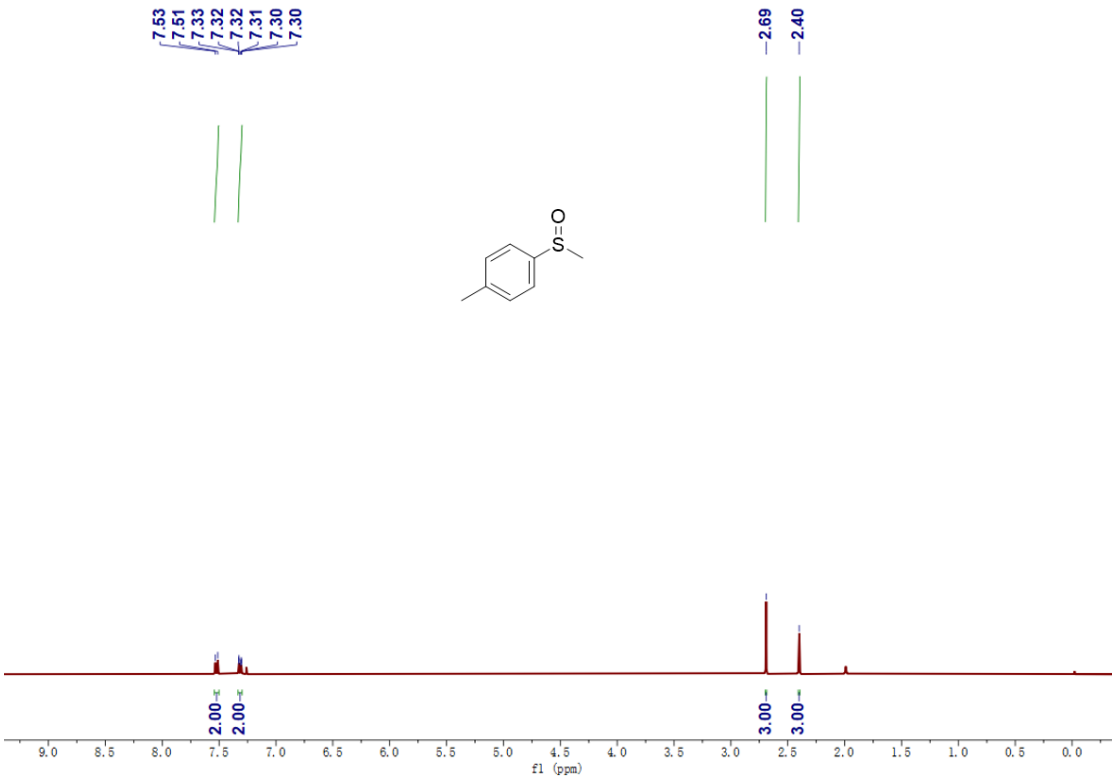

Fig. S15 ^{1}H NMR spectra of **2b** in $CDCl_3$.

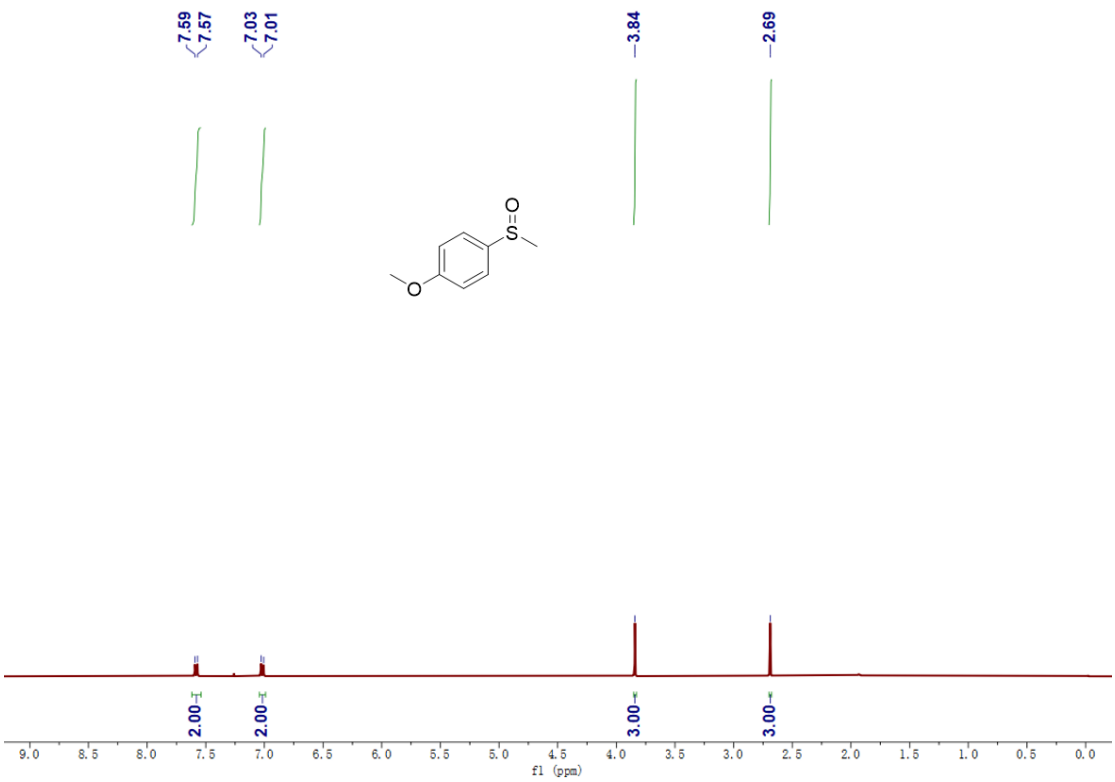

Fig. S16 ^{1}H NMR spectra of **2c** in $CDCl_3$.

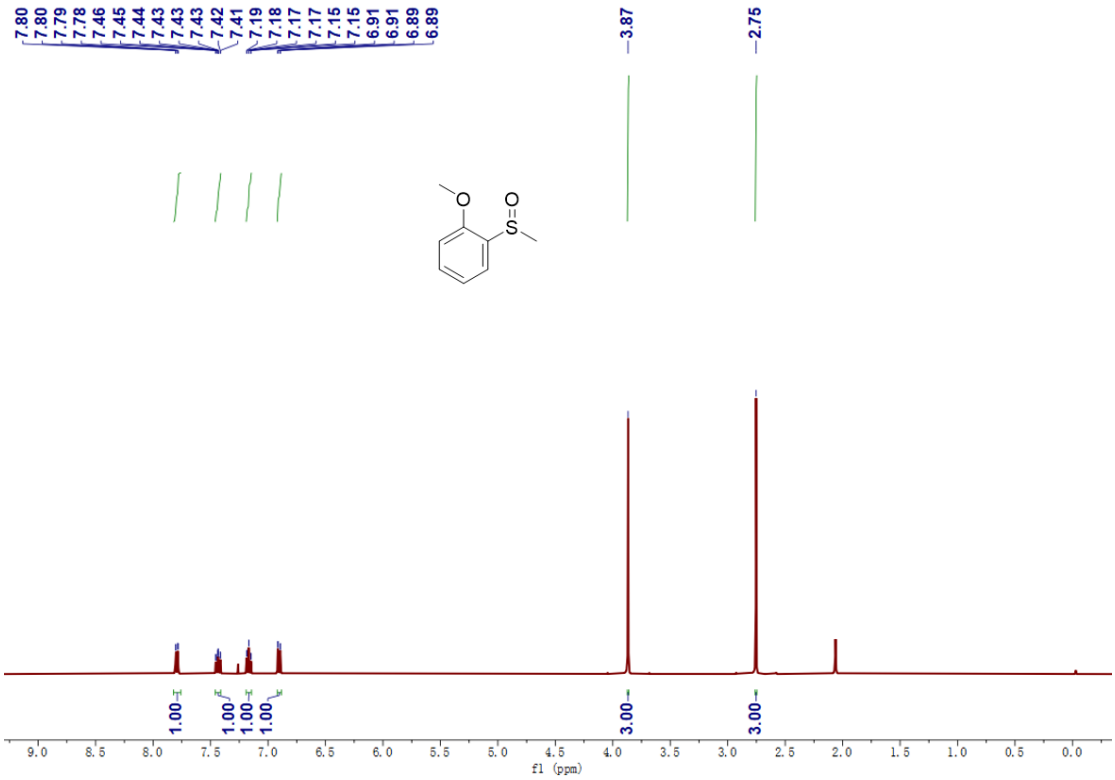

Fig. S17 ^{1}H NMR spectra of **2d** in $CDCl_3$.

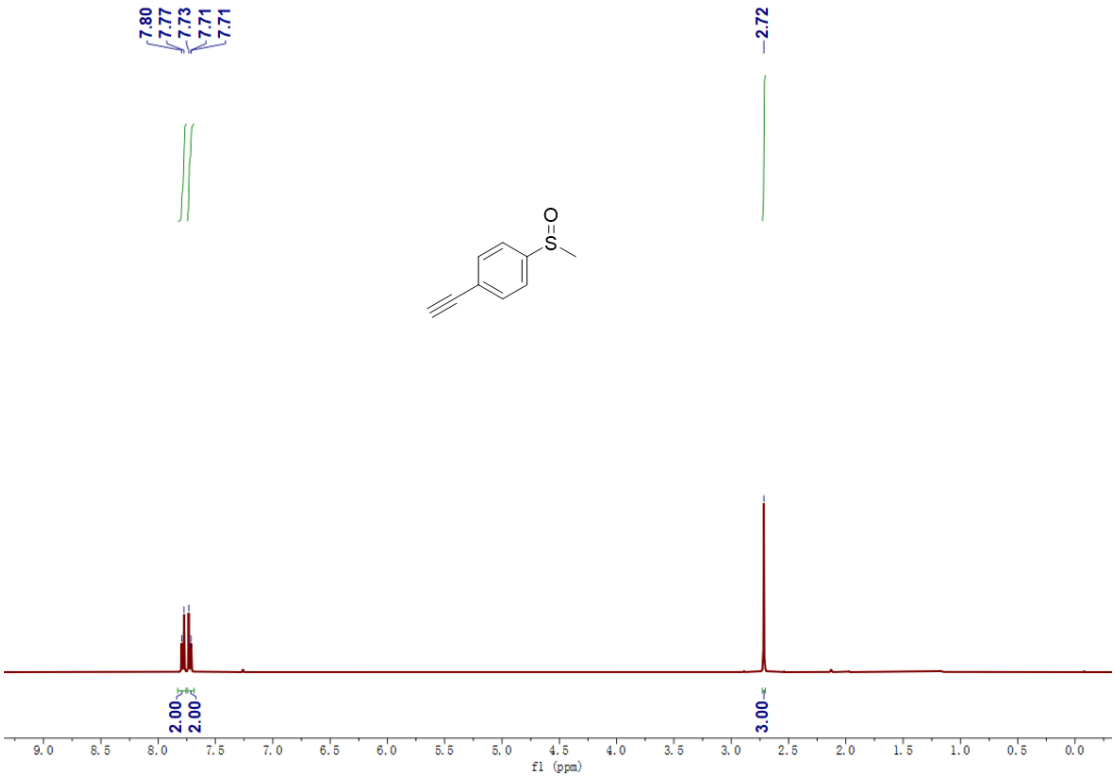

Fig. S18 ^{1}H NMR spectra of **2e** in $CDCl_3$.

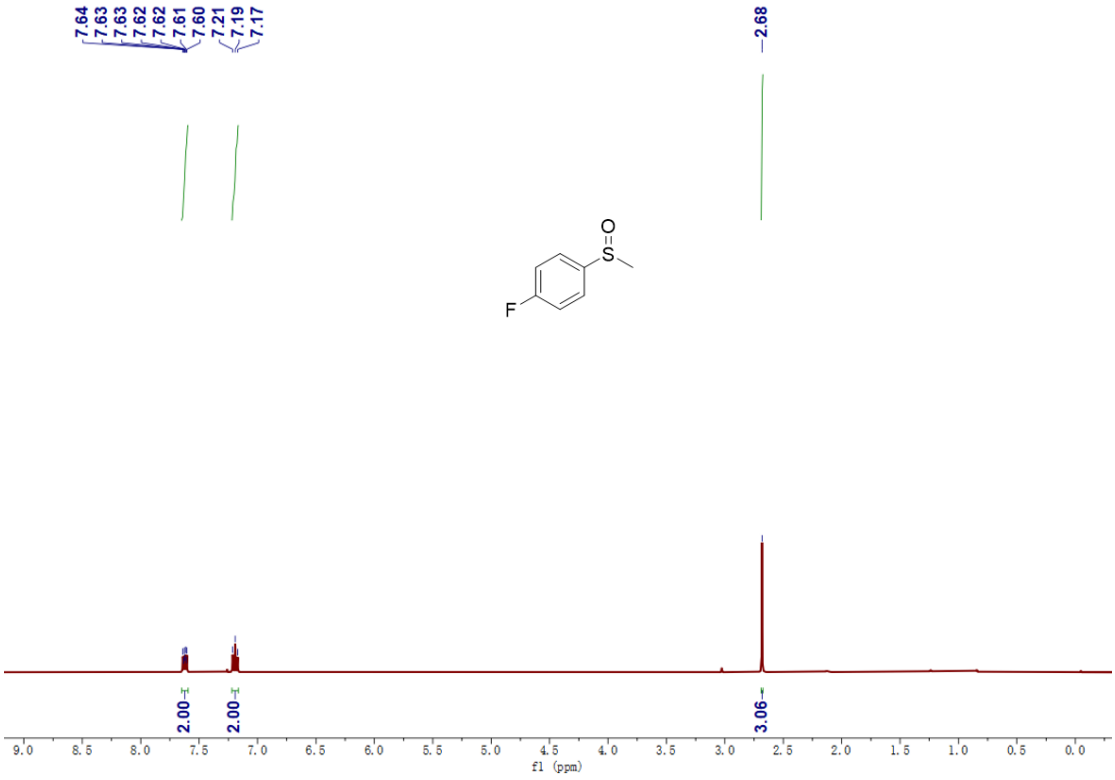

Fig. S19 ^{1}H NMR spectra of **2f** in $CDCl_3$.

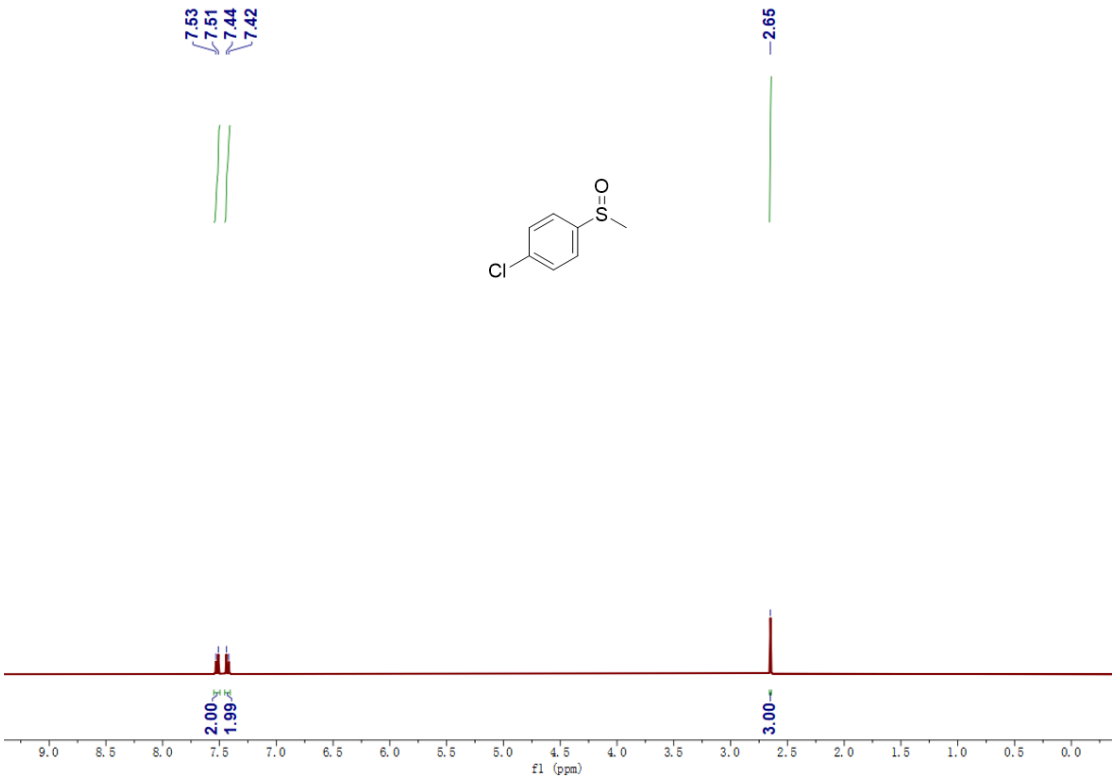

Fig. S20 ^{1}H NMR spectra of **2g** in $CDCl_3$.

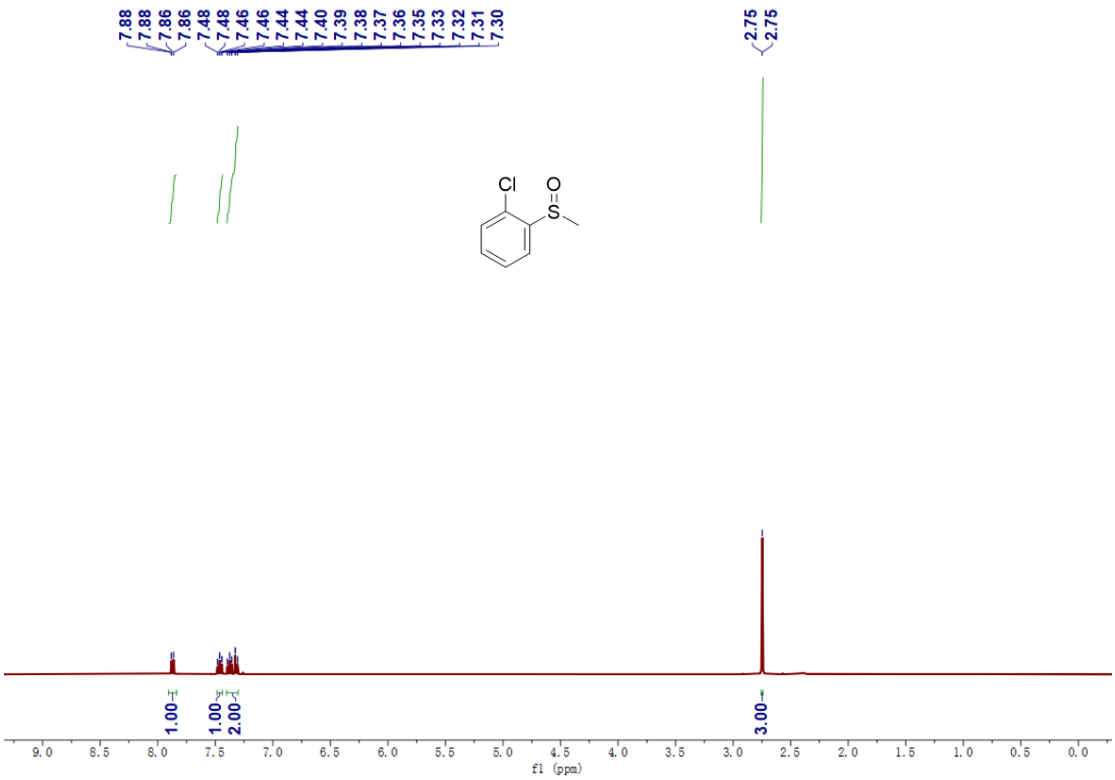

Fig. S21 ^{1}H NMR spectra of **2h** in $CDCl_3$.

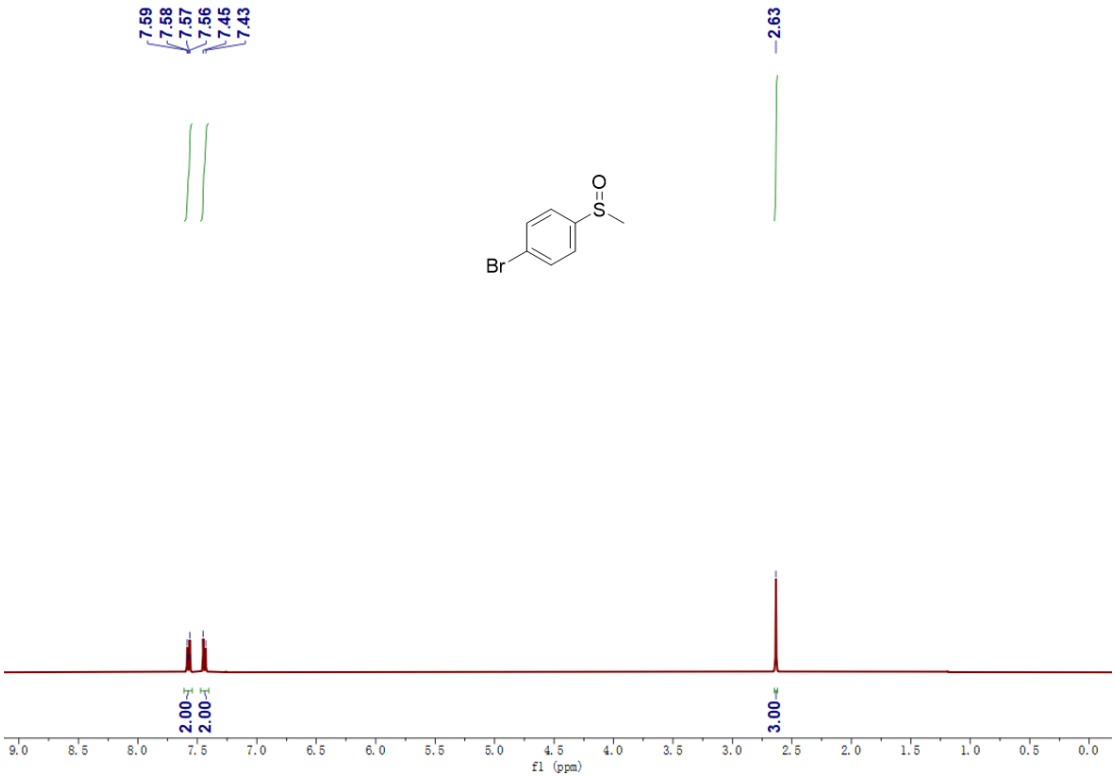

Fig. S22 ^{1}H NMR spectra of **2i** in $CDCl_3$.

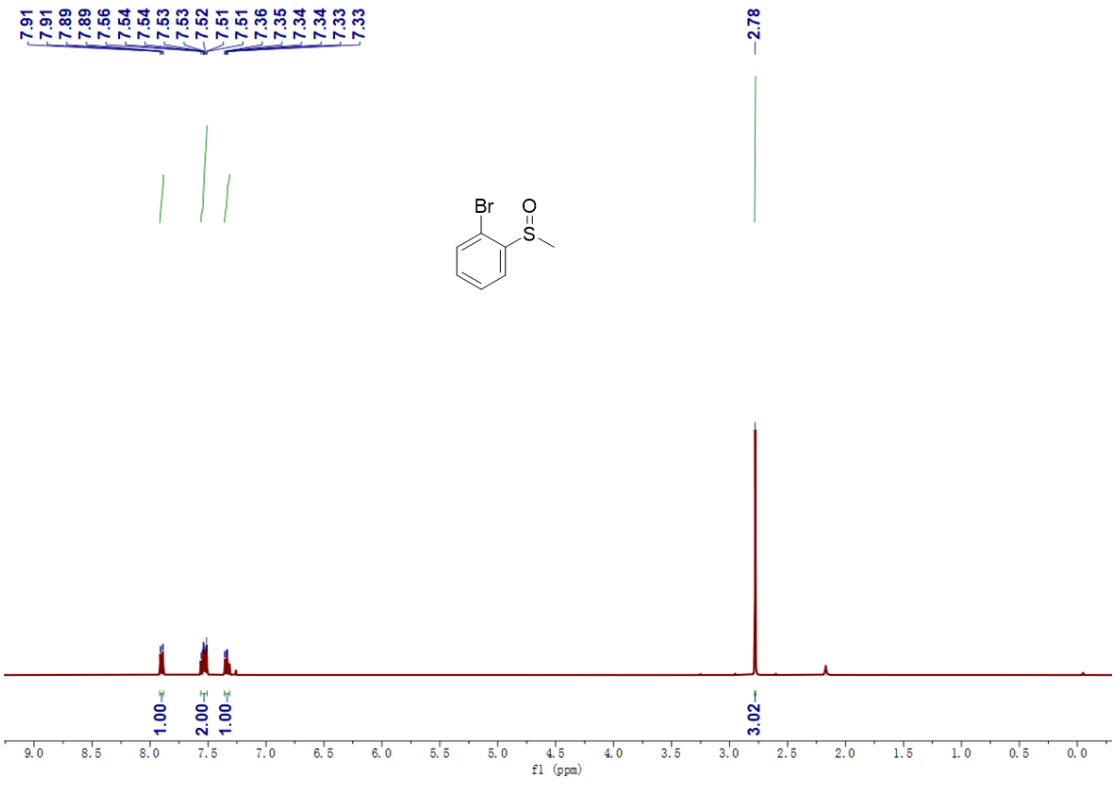

Fig. S23 ^{1}H NMR spectra of **2j** in $CDCl_3$.

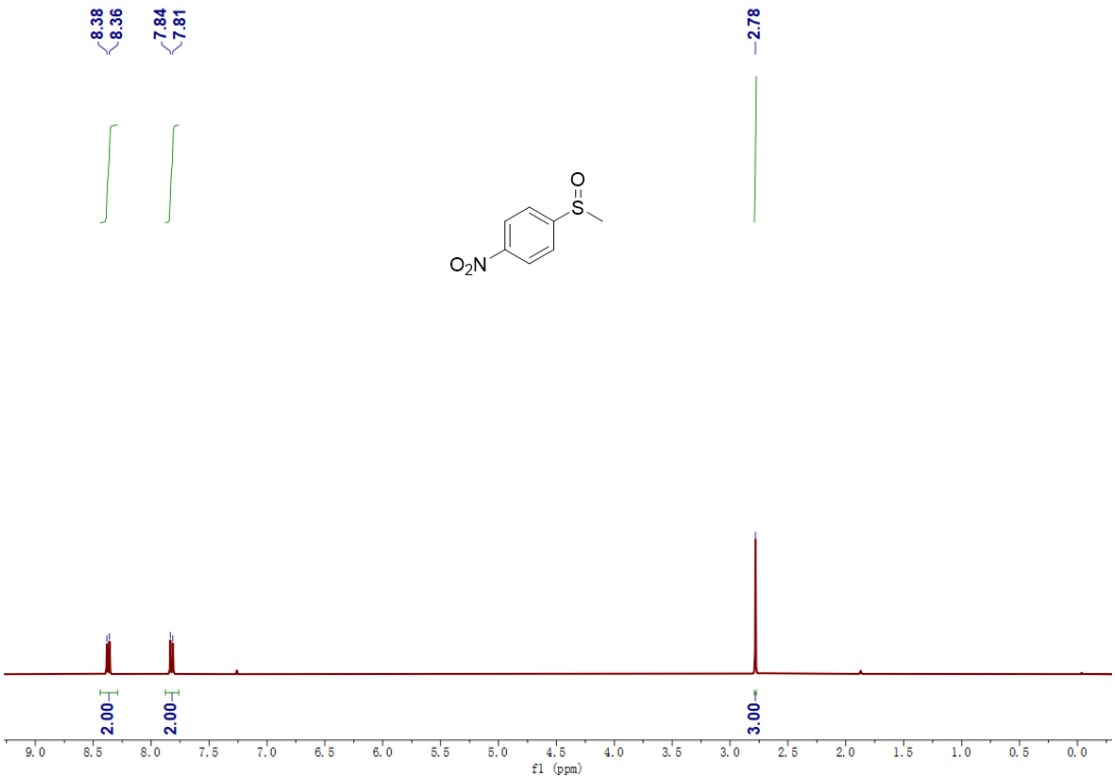

Fig. S24 ^{1}H NMR spectra of **2k** in $CDCl_3$.

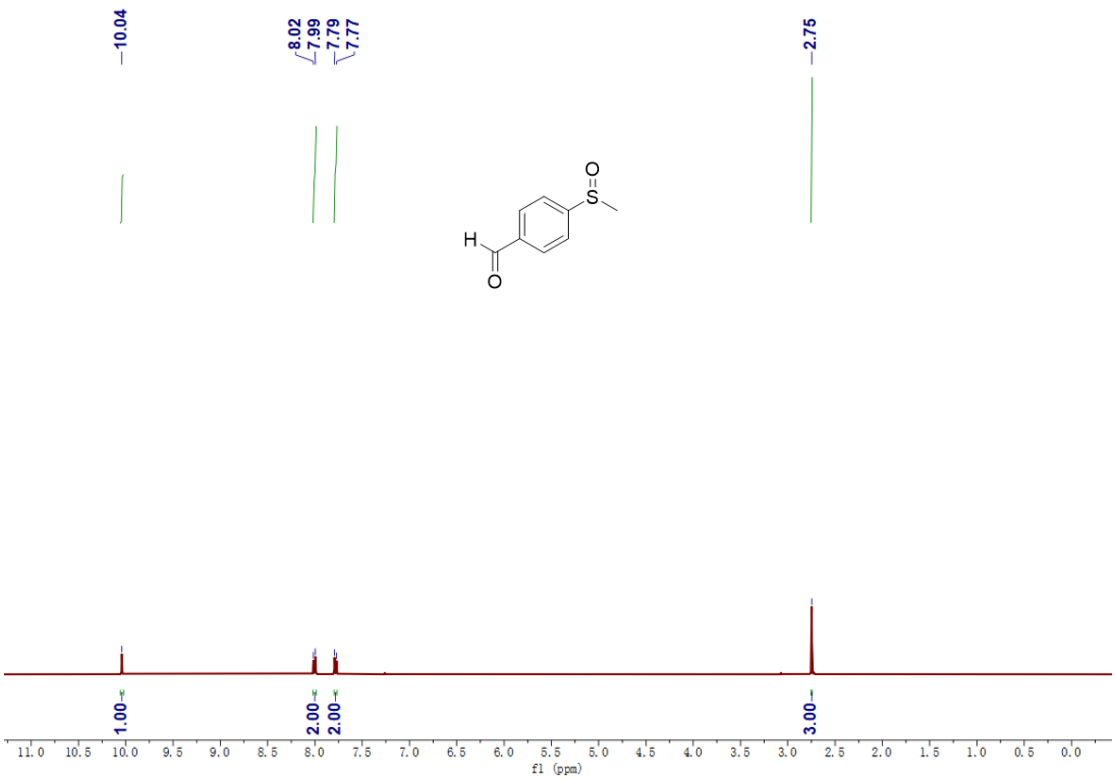

Fig. S25 ^{1}H NMR spectra of **2l** in $CDCl_3$.

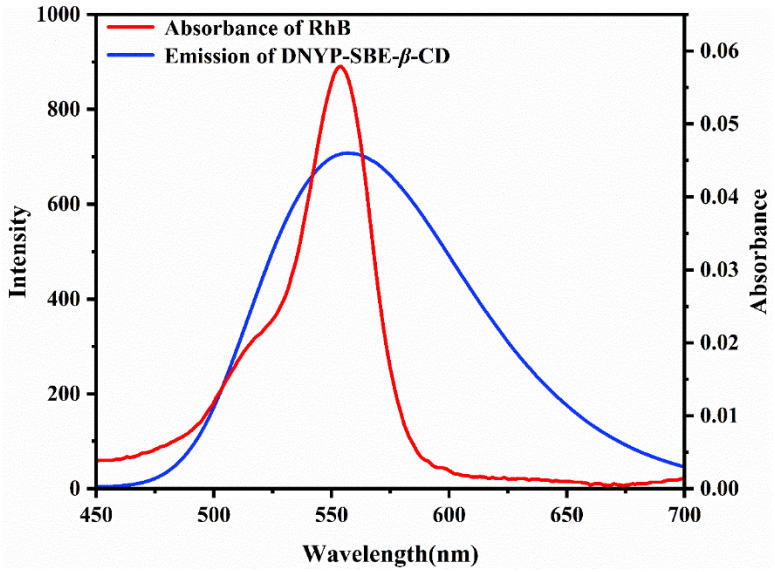

Fig. S26 The UV-vis absorption spectra of RhB and the fluorescence emission spectra of DNPY-SBE-β-CD. [DNPY] = 1.0×10^{-5} mol/L, [SBE-β-CD] = 2.0×10^{-6} mol/L, [RhB] = 1.0×10^{-6} mol/L.

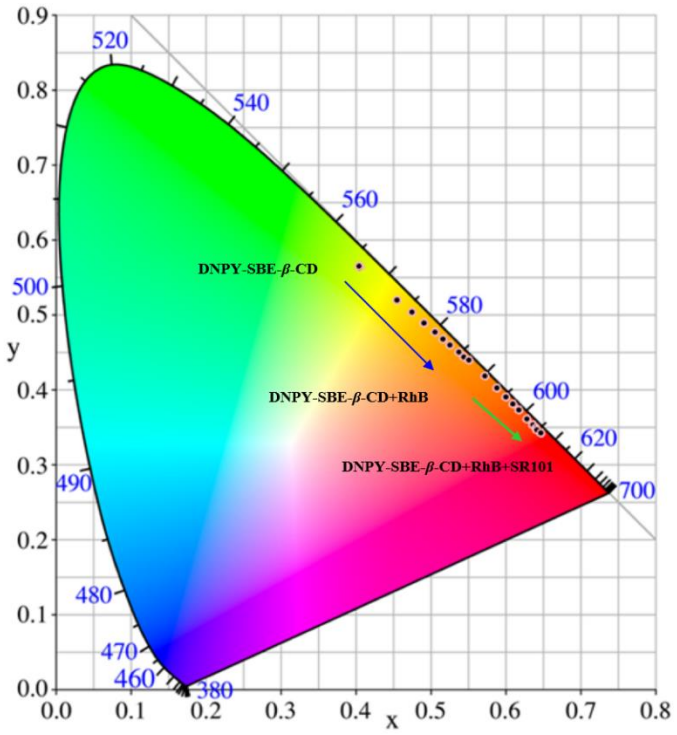

Fig. S27 CIE chromaticity coordinates of DNPY-SBE-β-CD at different concentrations of RhB (from 0 to 0.1 equiv.) and SR101 (from 0 to 0.10 equiv.). [DNPY] = 1.0×10^{-5} mol/L, [SBE-β-CD] = 2.0×10^{-6} mol/L, [RhB] = 1.0×10^{-6} mol/L, [SR101] = 1.0×10^{-6} mol/L.

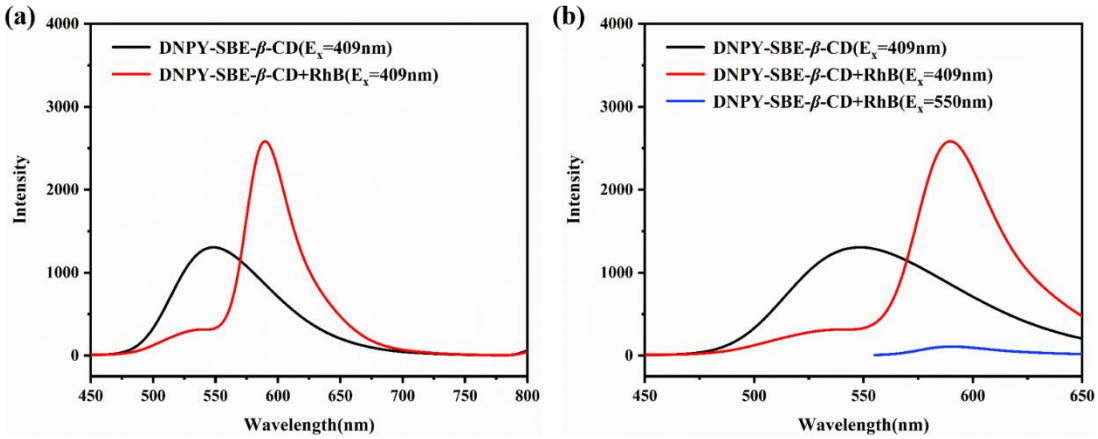

Fig. S28 (a) Fluorescence emission spectra of DNPY-SBE-β-CD and DNPY-SBE-β-CD+RhB; (b) Fluorescence emission spectra of DNPY-SBE-β-CD+RhB (the red line), DNPY-SBE-β-CD+RhB (the blue line), DNPY-SBE-β-CD (the black line). [DNPY] = 1.0×10^{-5} mol/L, [SBE-β-CD] = 2.0×10^{-6} mol/L, [RhB] = 1.0×10^{-6} mol/L, [SR101] = 1.0×10^{-6} mol/L.

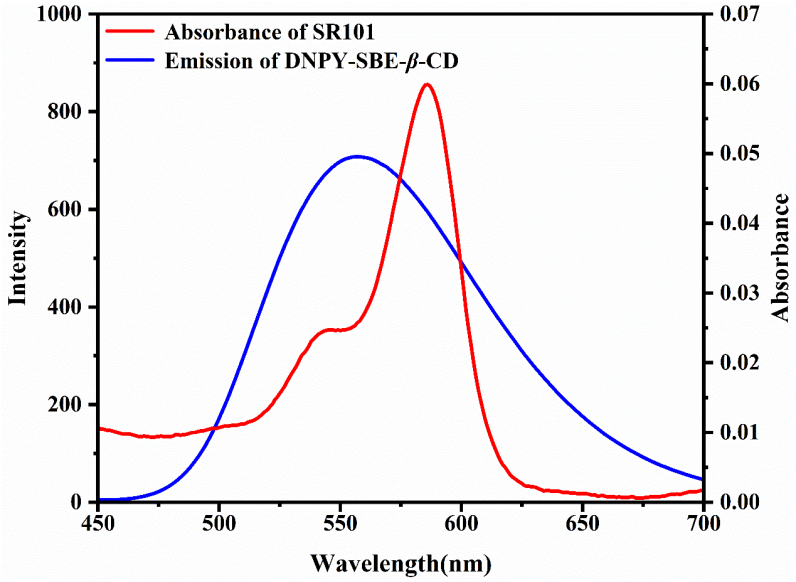

Fig. S29 The UV-vis absorption spectra of SR101 and the fluorescence emission spectra of DNPY-SBE-β-CD+RhB. [DNPY] = 1.0×10^{-5} mol/L, [SBE-β-CD] = 2.0×10^{-6} mol/L, [RhB] = 1.0×10^{-6} mol/L, [SR101] = 1.0×10^{-6} mol/L.

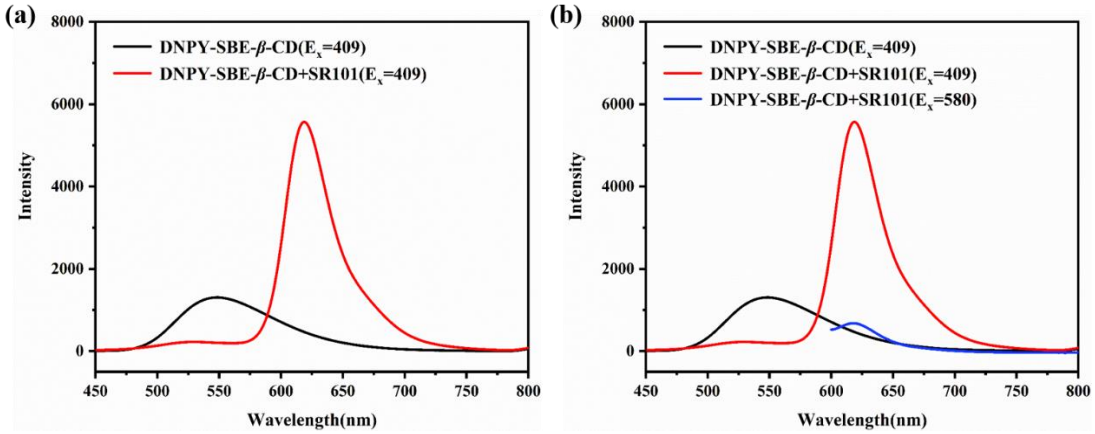

Fig. S30 (a) Fluorescence emission spectra of DNPY-SBE-β-CD+RhB and DNPY-SBE-β-CD+RhB+SR101; (b) Fluorescence emission spectra of DNPY-SBE-β-CD+RhB+SR101 (the red line), DNPY-SBE-β-CD+RhB+SR101 (the blue line), DNPY-SBE-β-CD+RhB (the black line). [DNPY] = 1.0×10^{-5} mol/L, [SBE-β-CD] = 2.0×10^{-6} mol/L, [RhB] = 1.0×10^{-6} mol/L, [SR101] = 1.0×10^{-6} mol/L.

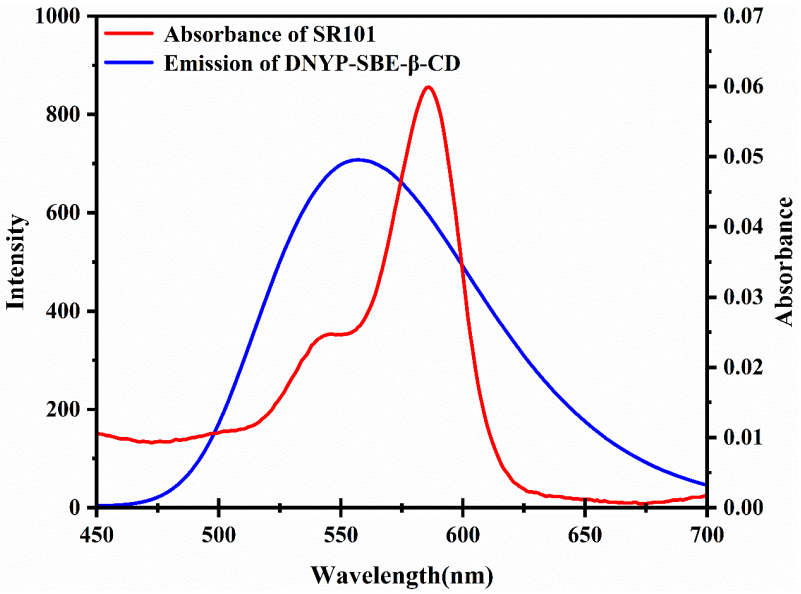

Fig. S31 The UV-vis absorption spectra of SR101 and the fluorescence emission spectra (λ_{ex} = 409 nm) of DNPY-SBE-β-CD. [DNPY] = 1.0×10^{-5} mol/L, [SBE-β-CD] = 2.0×10^{-6} mol/L, [SR101] = 1.0×10^{-6} mol/L.

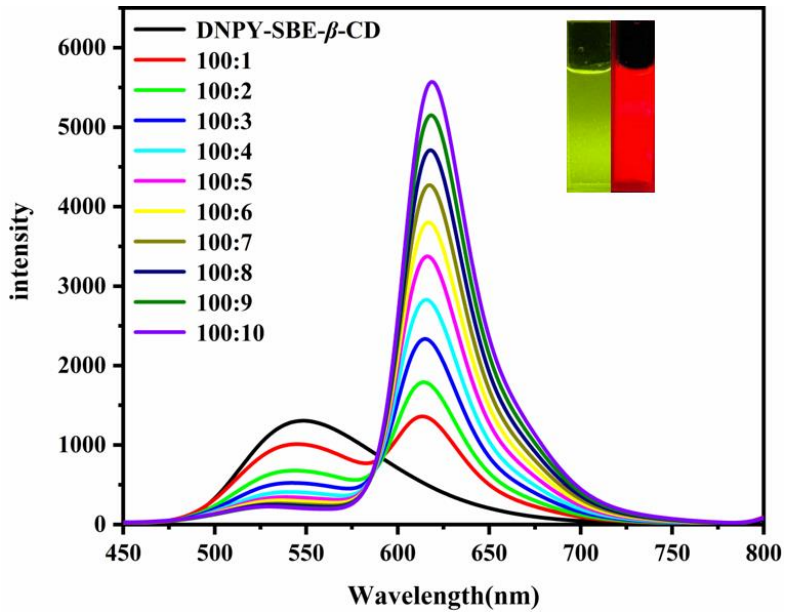

Fig. S32 Fluorescence emission spectra of DNPY-SBE-β-CD with addition of SR101 in aqueous solution. (Inset: Fluorescence emission colour of DNPY-SBE-β-CD before and after addition of SR101). [DNPY] = 1.0×10^{-5} mol/L, [SBE-β-CD] = 2.0×10^{-6} mol/L, [SR101] = 1.0×10^{-6} mol/L.

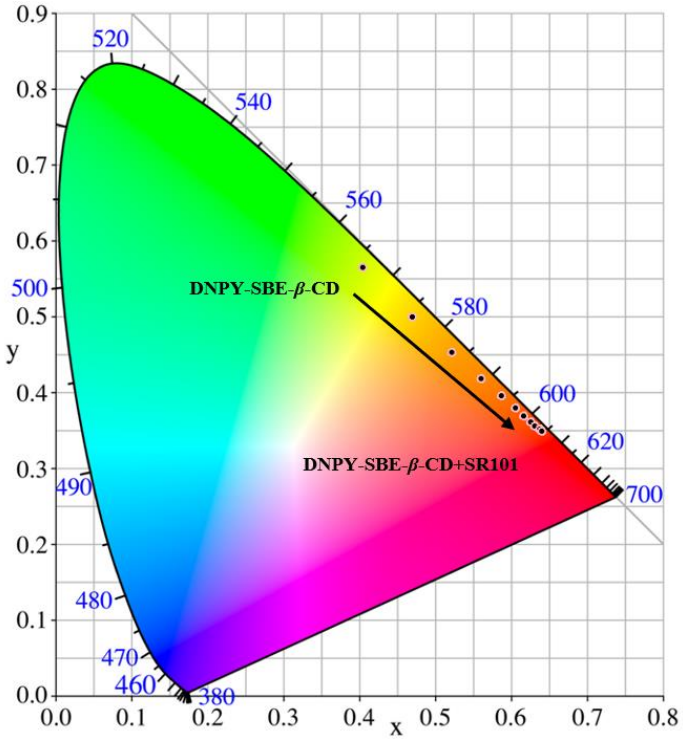

Fig. S33 CIE chromaticity coordinates of DNPY-SBE-β-CD at different concentrations of SR101 (from 0 to 0.10 equiv.). [DNPY] = 1.0×10^{-5} mol/L, [SBE-β-CD] = 2.0×10^{-6} mol/L, [SR101] = 1.0×10^{-6} mol/L.

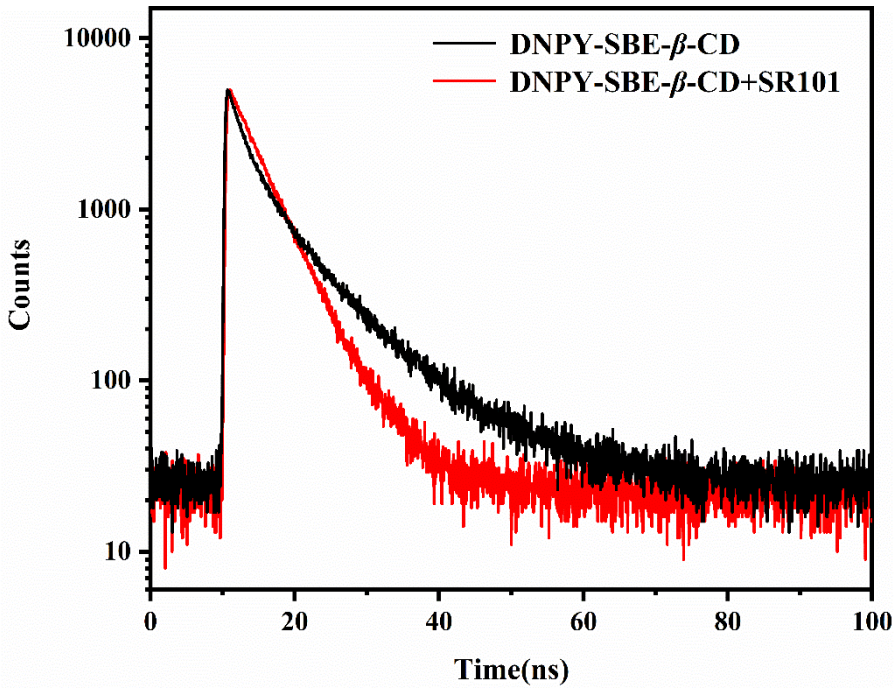

Fig. S34 Time-resolved fluorescence decay curves of DNPY-SBE-β-CD and DNPY-SBE-β-CD +SR101. [DNPY] = 1.0×10^{-5} mol/L, [SBE-β-CD] = 2.0×10^{-6} mol/L, [SR101] = 1.0×10^{-6} mol/L.

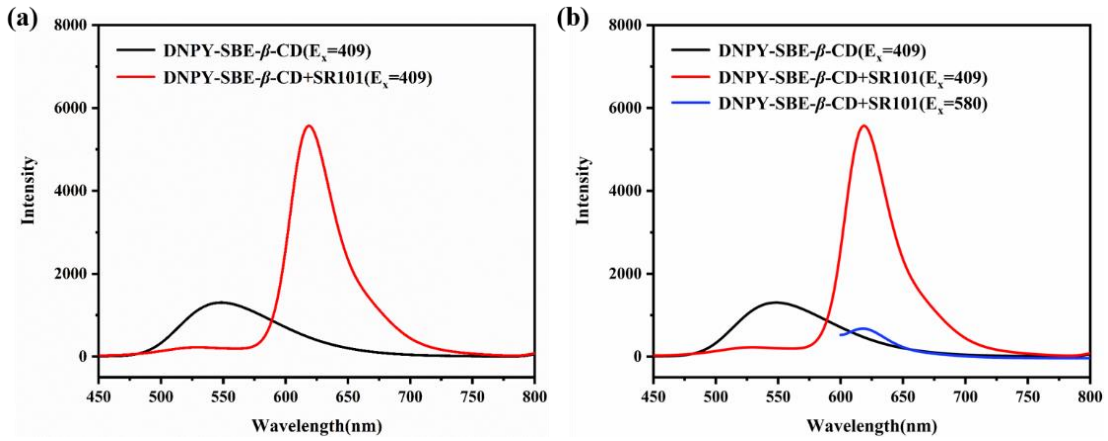

Fig. S35 (a) Fluorescence emission spectra of DNPY-SBE-β-CD and DNPY-SBE-β-CD+SR101; (b) Fluorescence emission spectra of DNPY-SBE-β-CD+SR101 (the red line), DNPY-SBE-β-CD+SR101 (the blue line), DNPY-SBE-β-CD (the black line). [DNPY] = 1.0×10^{-5} mol/L, [SBE-β-CD] = 2.0×10^{-6} mol/L, [SR101] = 1.0×10^{-6} mol/L.

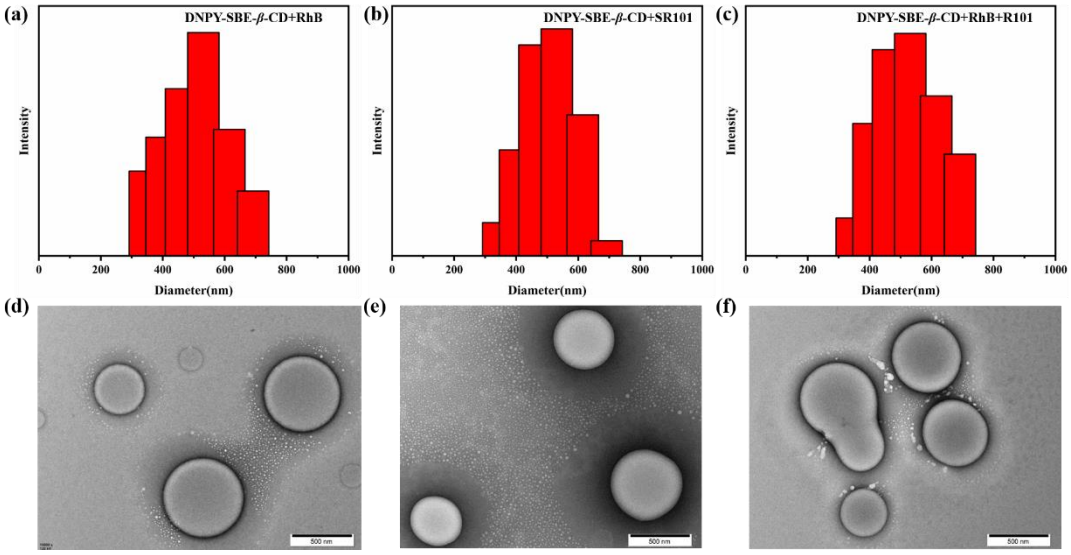

Fig. S36 DLS and TEM images of (a), (d) DNPY-SBE-β-CD+RhB and (b), (e) DNPY-SBE-β-CD+SR101 and (c), (f) DNPY-SBE-β-CD+RhB+SR101. [DNPY] = 1.0×10^{-5} mol/L, [SBE-β-CD] = 2.0×10^{-6} mol/L, [RhB] = 1.0×10^{-6} mol/L, [SR101] = 1.0×10^{-6} mol/L.

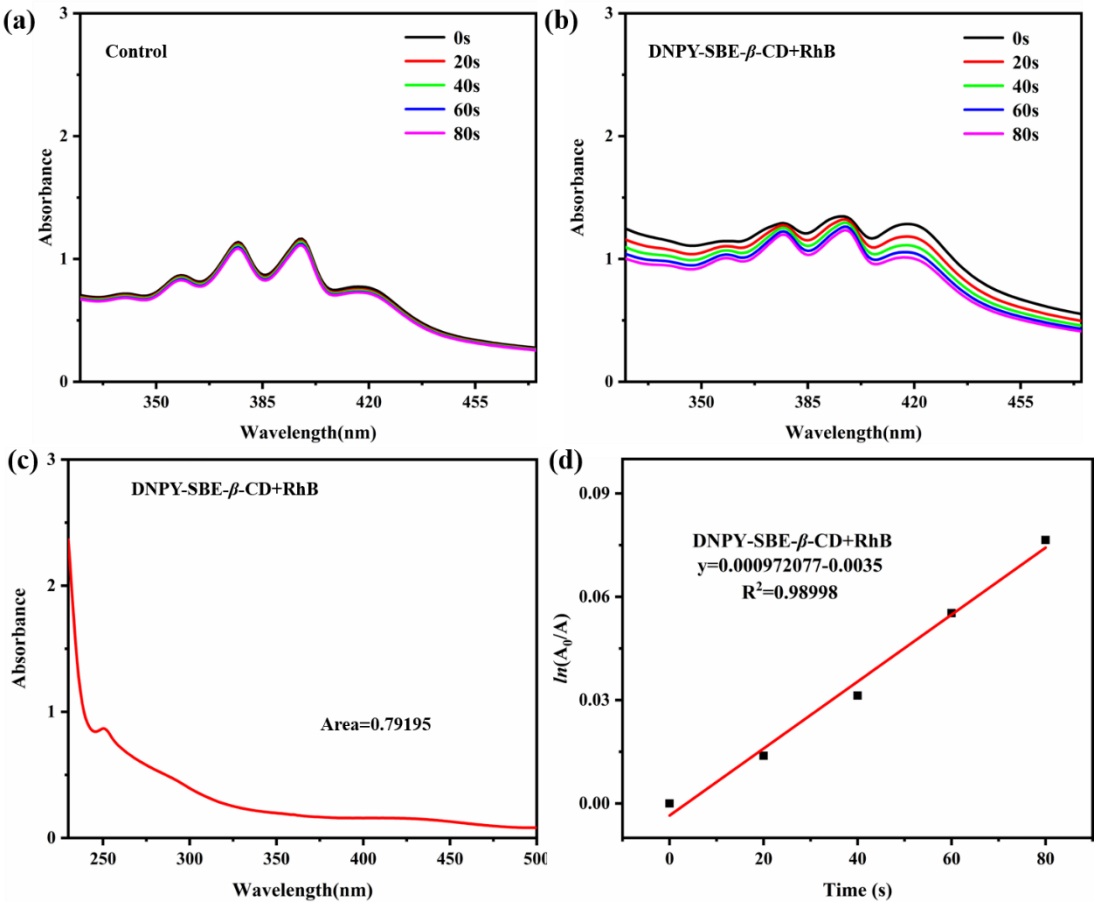

Fig. S37 The absorption spectra of ABDA after irradiation (410-415 nm, 10 W) for different time in the presence of (a) Control: ABDA without any additive; (b) DNPY-SBE-β-CD+RhB; (c) The UV-vis absorption spectra of DNPY-SBE-β-CD+RhB in the aqueous solution; (d) The decomposition rates of ABDA in the presence of DNPY-SBE-β-CD+RhB.

.

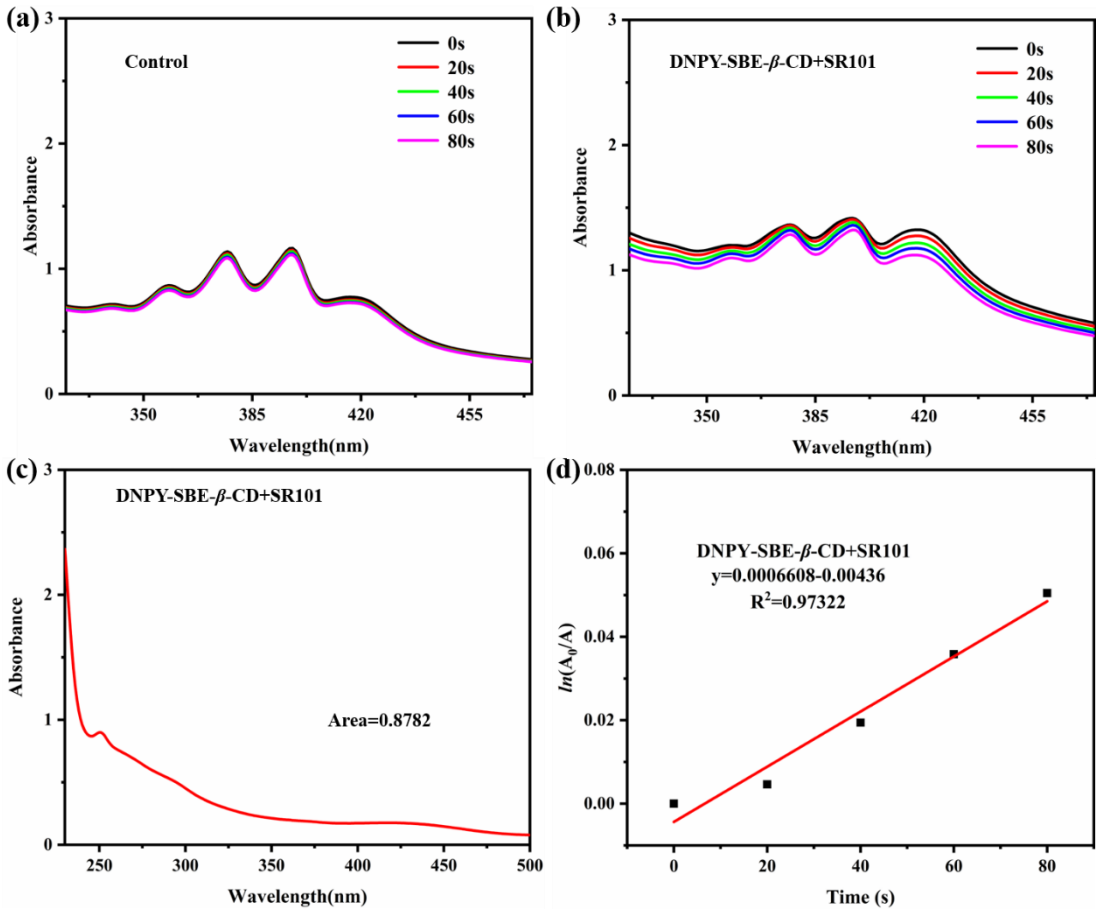

Fig. S38 The absorption spectra of ABDA after irradiation (410-415 nm, 10 W) for different time in the presence of (a) Control: ABDA without any additive; (b) DNPY-SBE-β-CD+SR101; (c) The UV-vis absorption spectra of DNPY-SBE-β-CD+SR101 in the aqueous solution; (d) The decomposition rates of ABDA in the presence of DNPY-SBE-β-CD+SR101.

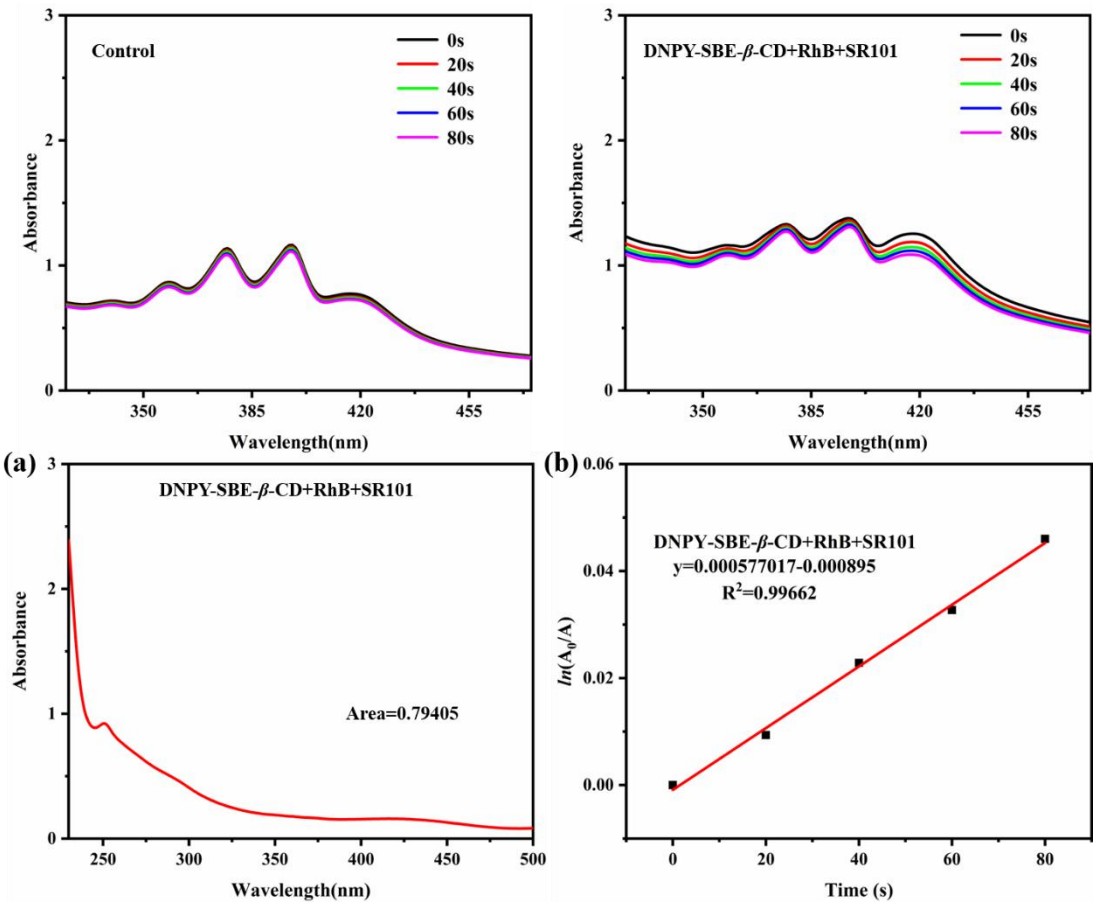

Fig. S39 The absorption spectra of ABDA after irradiation (410-415 nm, 10 W) for different time in the presence of (a) Control: ABDA without any additive; (b) DNPY-SBE-β-CD+RhB+SR101; (c) The UV-vis absorption spectra of DNPY-SBE-β-CD+RhB+SR101 in the aqueous solution; (d) The decomposition rates of ABDA in the presence of DNPY-SBE-β-CD+RhB+SR101.

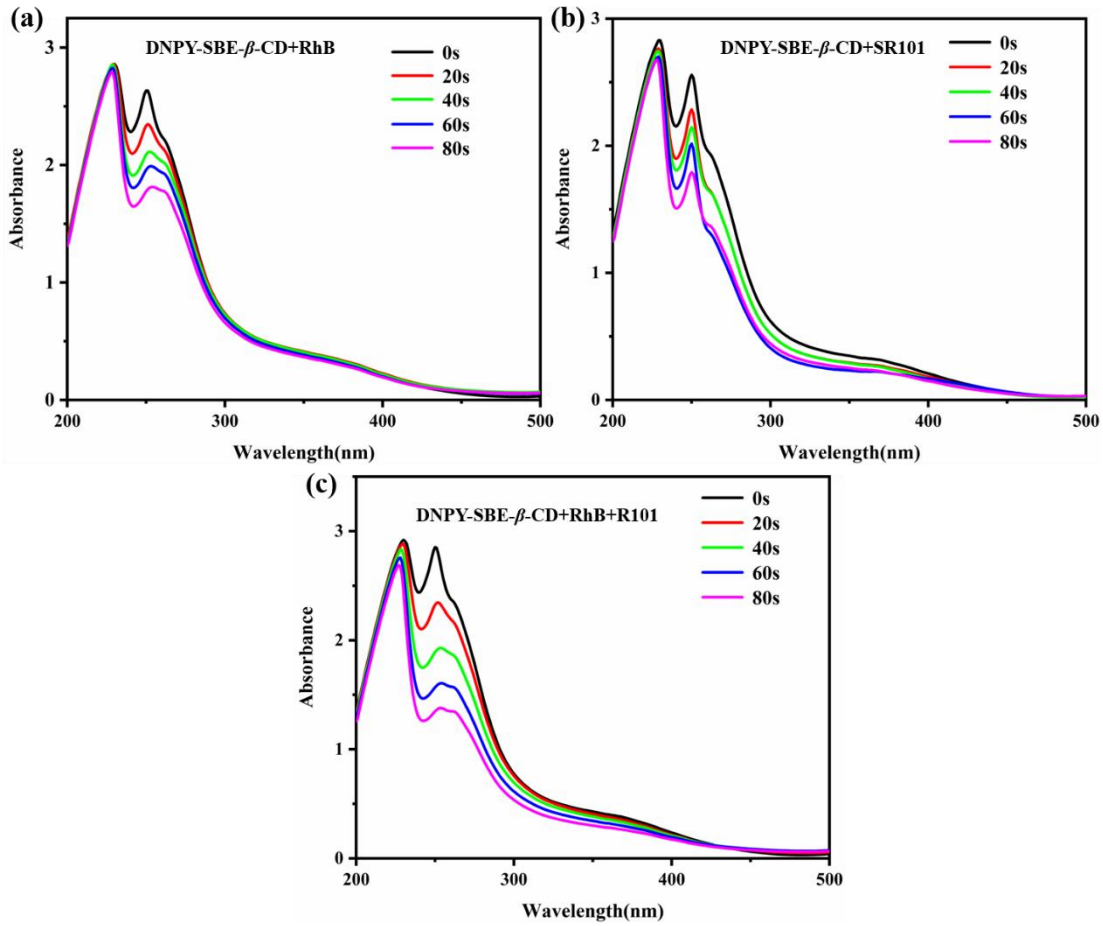

Fig. S40 The absorption spectra of NBT after irradiation (410-415 nm, 10 W) for different time in the presence of (a) DNPY-SBE-β-CD+RhB; (b) DNPY-SBE-β-CD+SR101; (c) DNPY-SBE-β-CD+RhB +SR101.

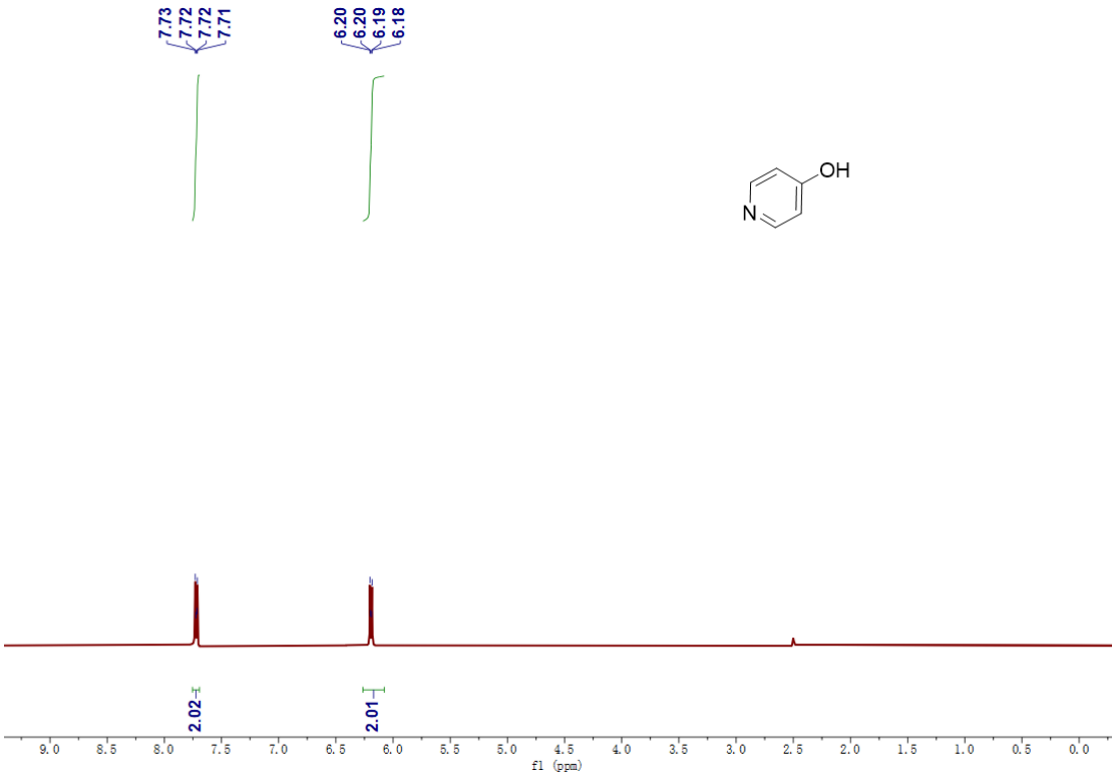

Fig. S41 ^{1}H NMR spectra of **4a** in DMSO-d_6.

Table S3 Oxidative hydroxylation of arylboronic acids with different base.[a, b]

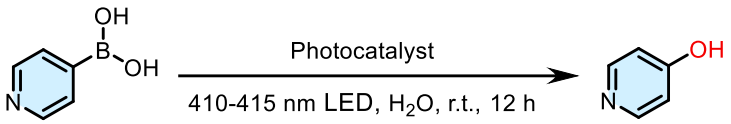

3 4a

Entry	Variation from standard conditions[a]	Yield[b][%]
1	None	93
2	DIPEA (0.2 mmol) instead of DIPEA (0.4 mmol)	75
3	Triethylamine (0.4 mmol) instead of DIPEA (0.4 mmol)	88
4	Trimethylamine(0.4 mmol) instead of DIPEA (0.4 mmol)	72

[a]Reaction conditions: 4-pyridylboronic acid (0.1 mmol), DIPEA (0.4 mmol), DNPY-SBE-β-CD+RhB+SR101 aqueous solution (0.5 mmol%, 3 mL), 410-415 nm LED, room temperature, 12 h; [b]Isolated yields.

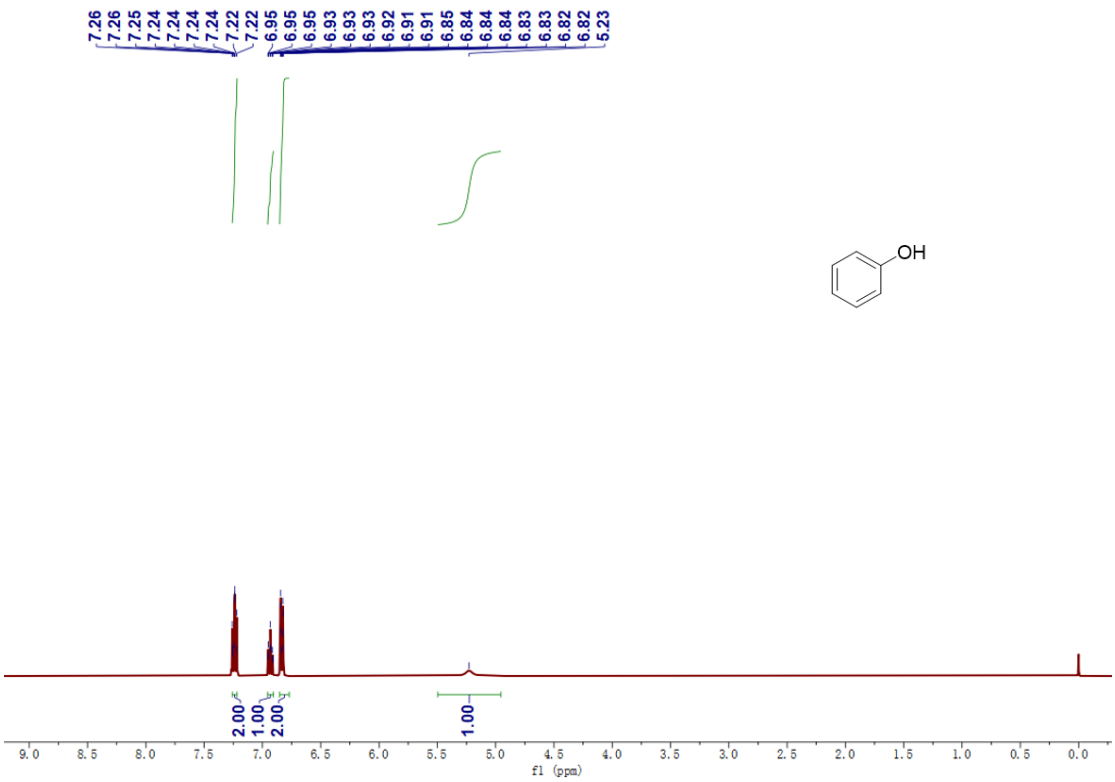

Fig. S42 ^{1}H NMR spectra of **4b** in $CDCl_3$.

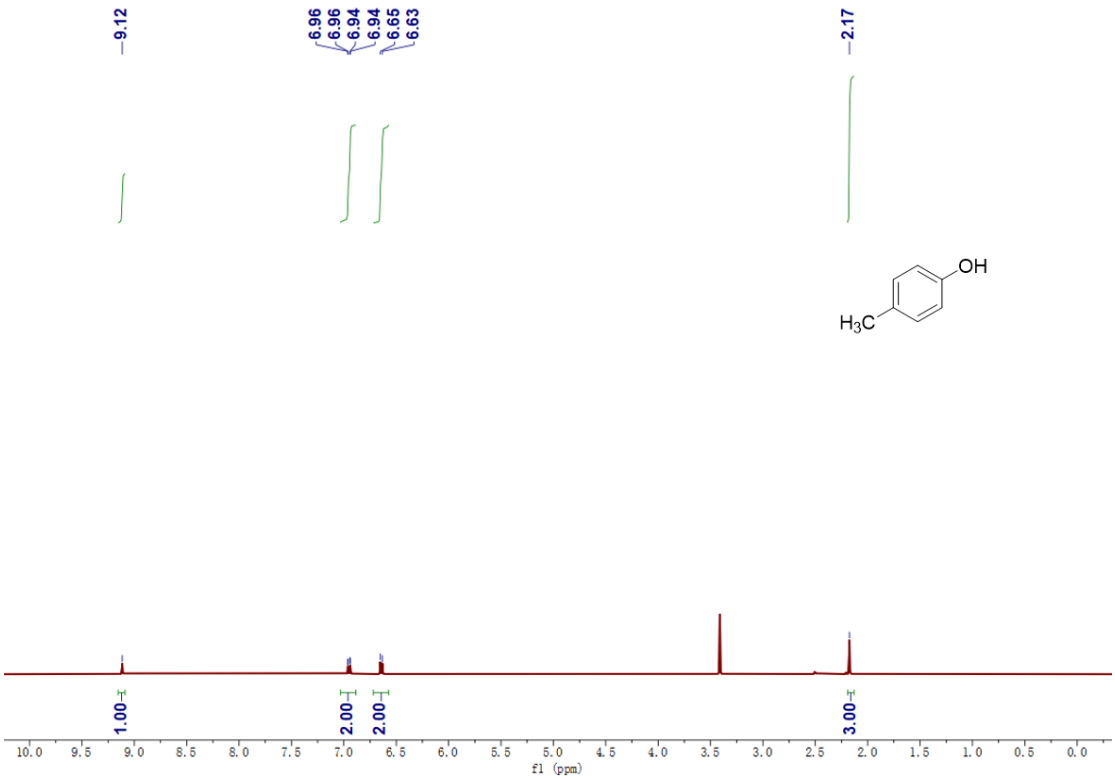

Fig. S43 ^{1}H NMR spectra of **4c** in DMSO-d_6.

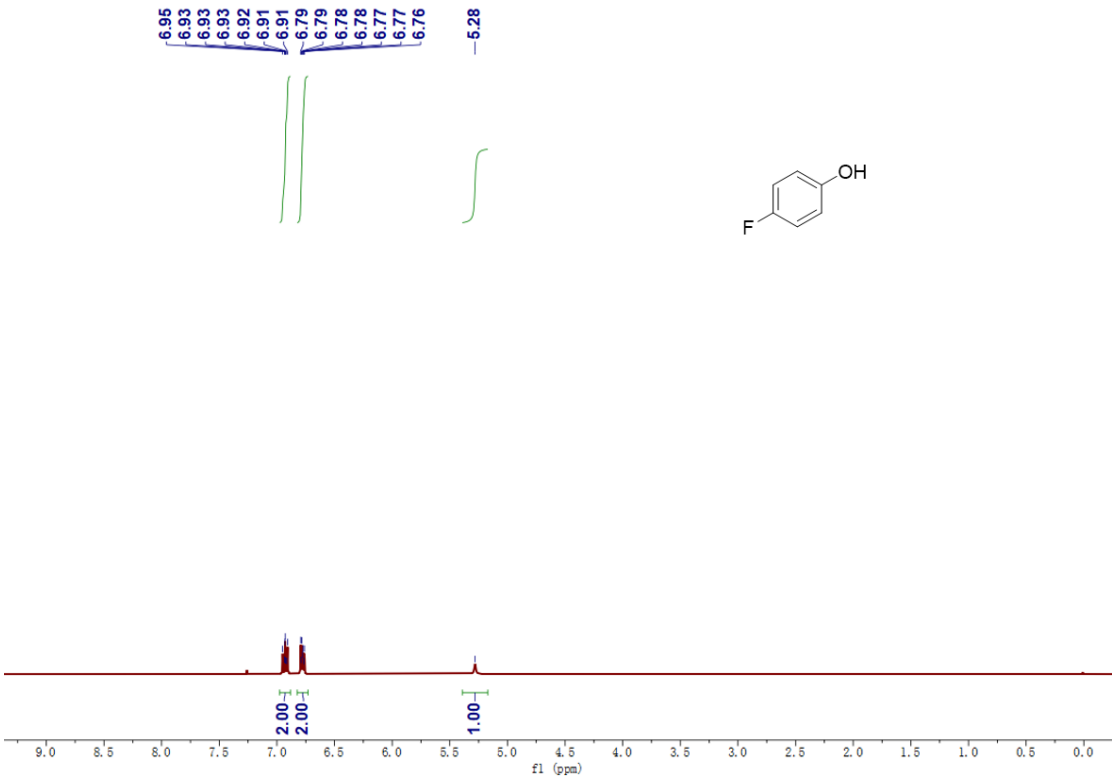

Fig. S44 ^{1}H NMR spectra of **4d** in $CDCl_3$.

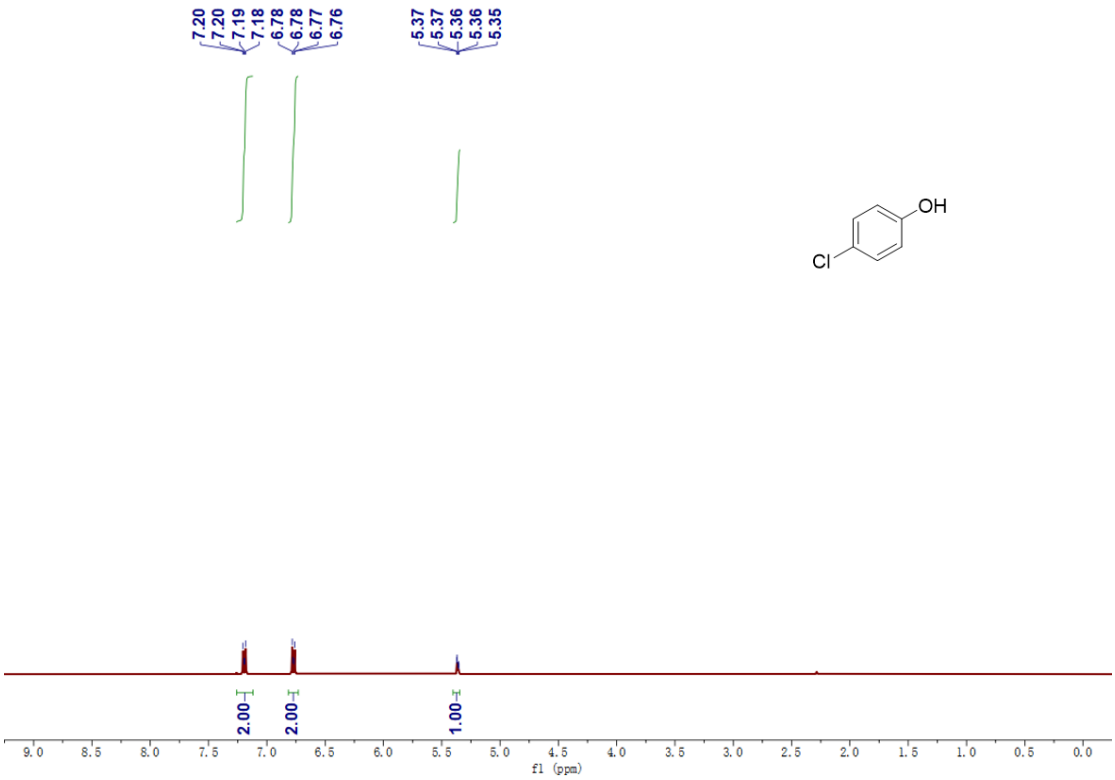

Fig. S45 ^{1}H NMR spectra of **4e** in $CDCl_3$.

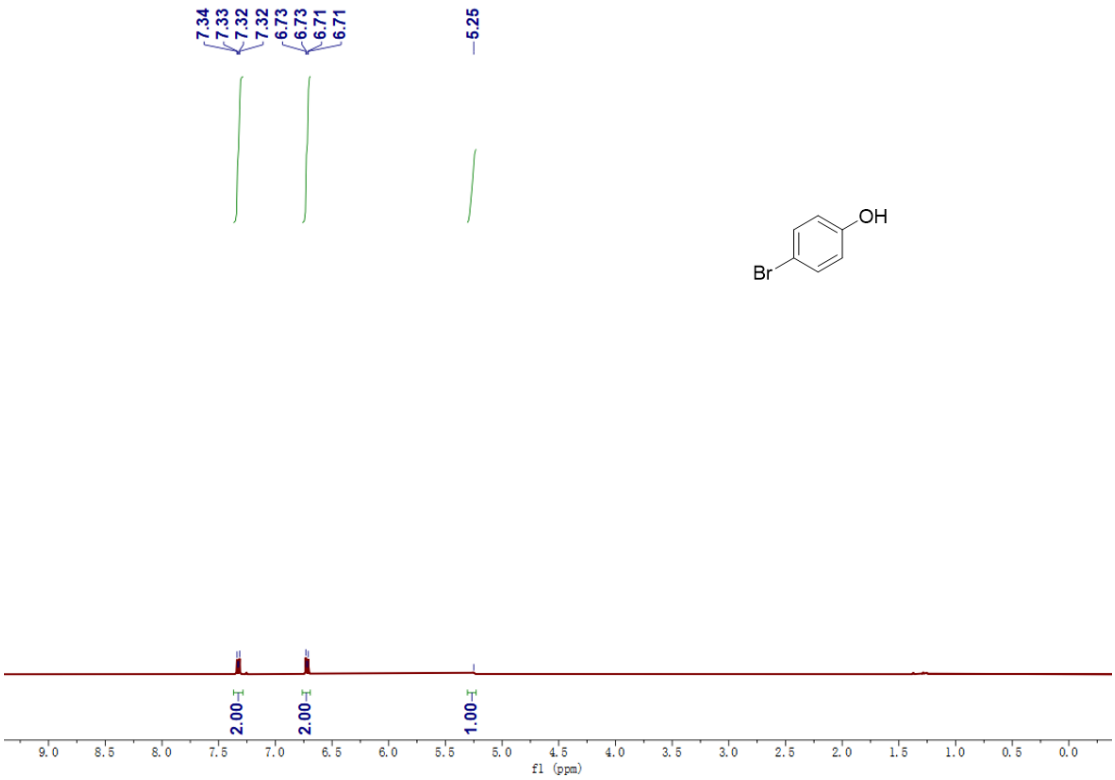

Fig. S46 ^{1}H NMR spectra of **4f** in $CDCl_3$.

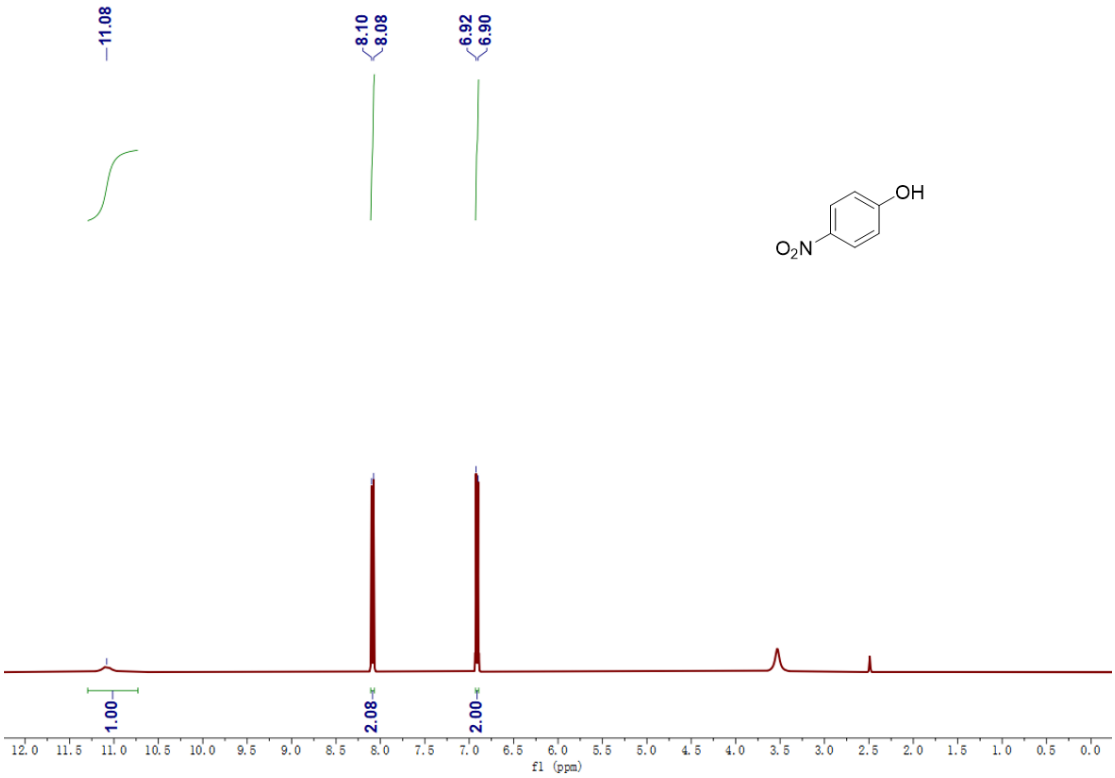

Fig. S47 ^{1}H NMR spectra of **4g** in DMSO-d_6.

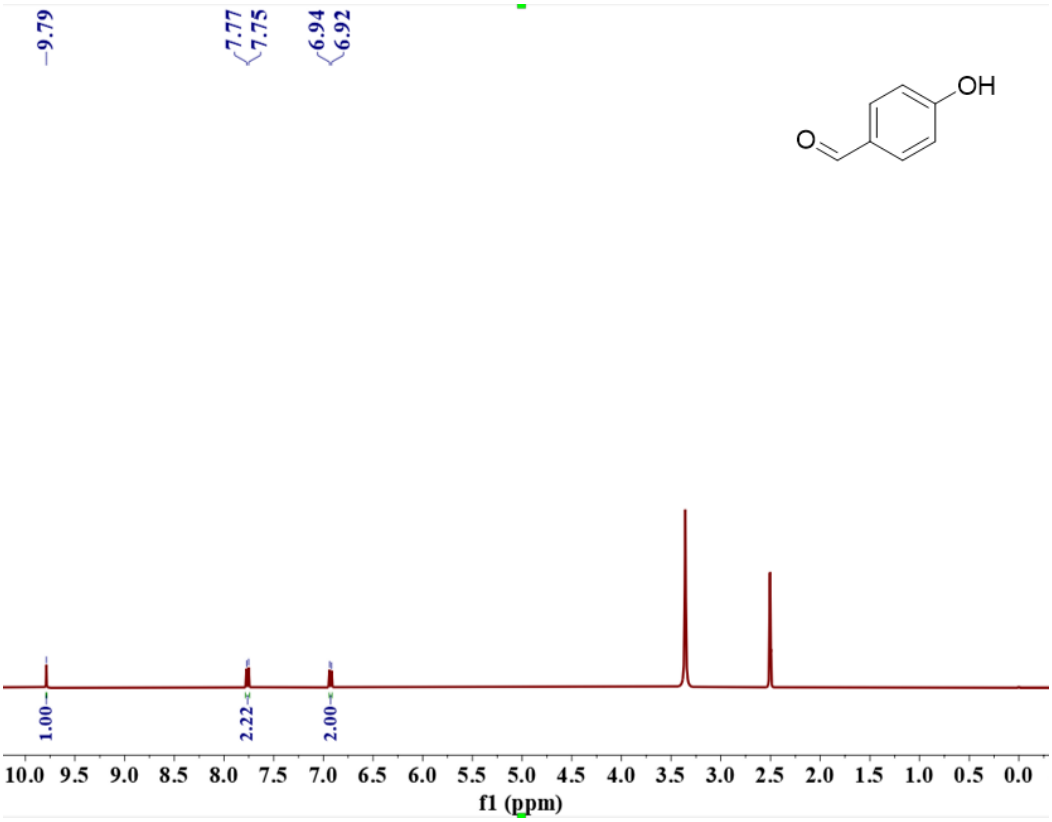

Fig. S48 ^{1}H NMR spectra of **4h** in DMSO-d_6.

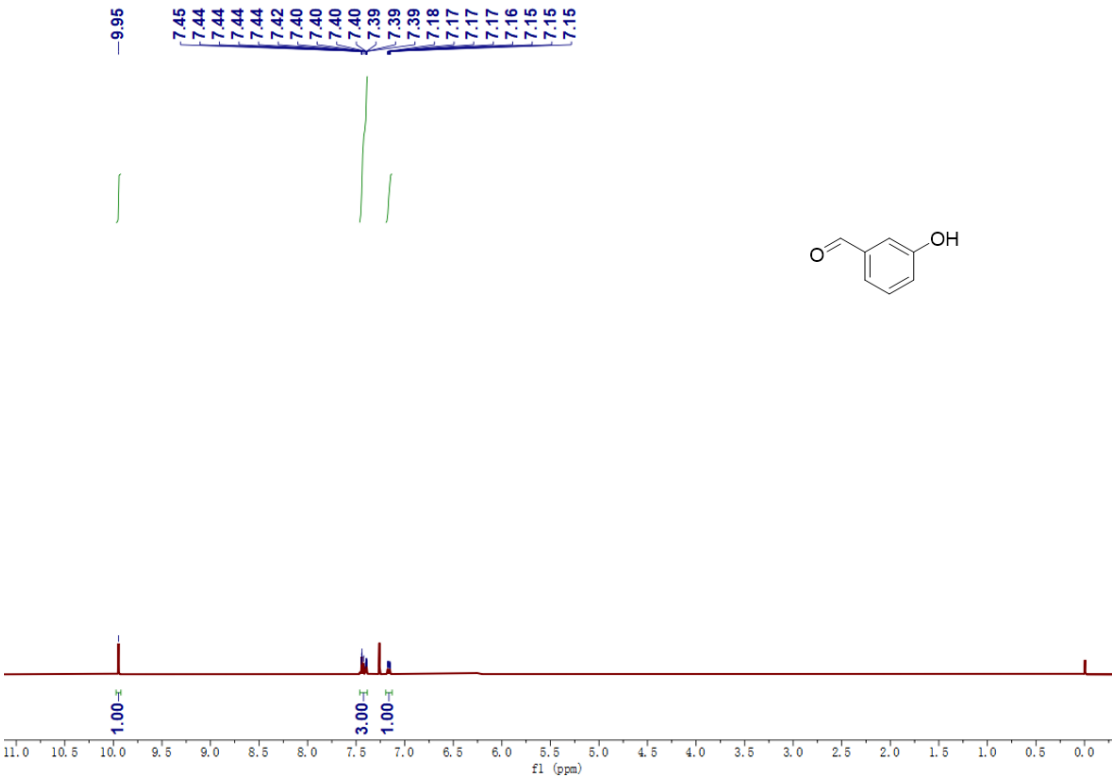

Fig. S49 ^{1}H NMR spectra of **4i** in $CDCl_3$.

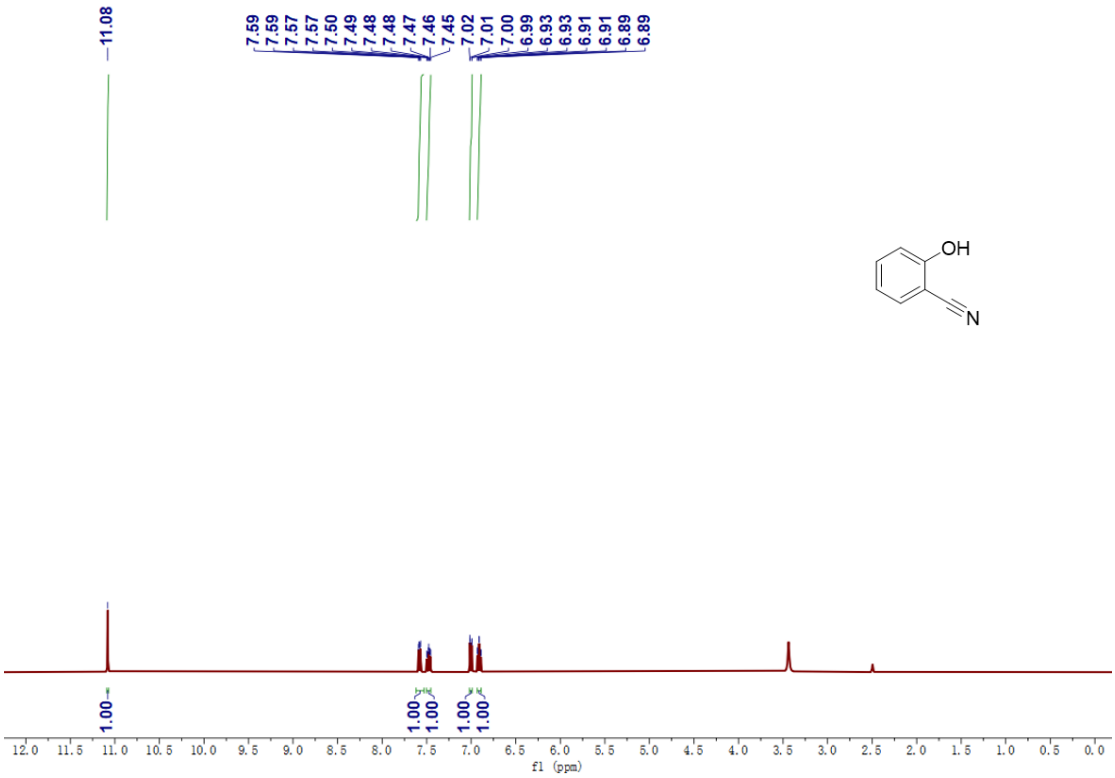

Fig. S50 ^{1}H NMR spectra of **4j** in DMSO-d_6.

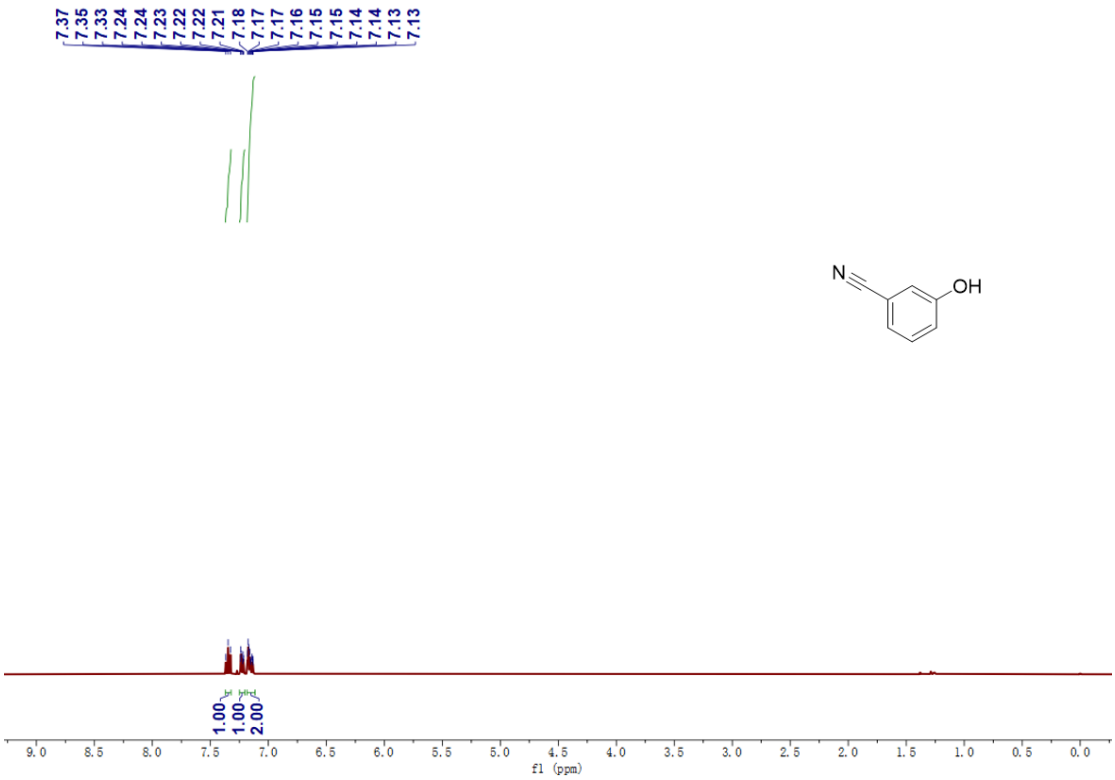

Fig. S51 ^{1}H NMR spectra of **4k** in $CDCl_3$.

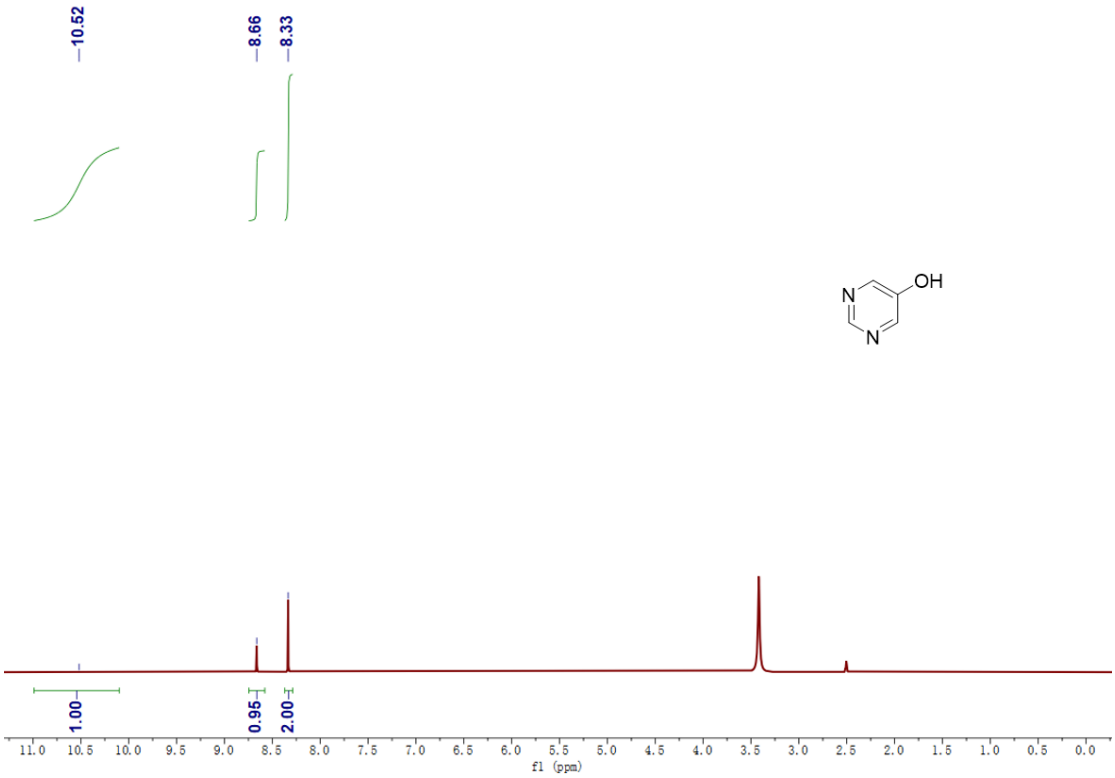

Fig. S52 ^{1}H NMR spectra of **4l** in DMSO-d_6.

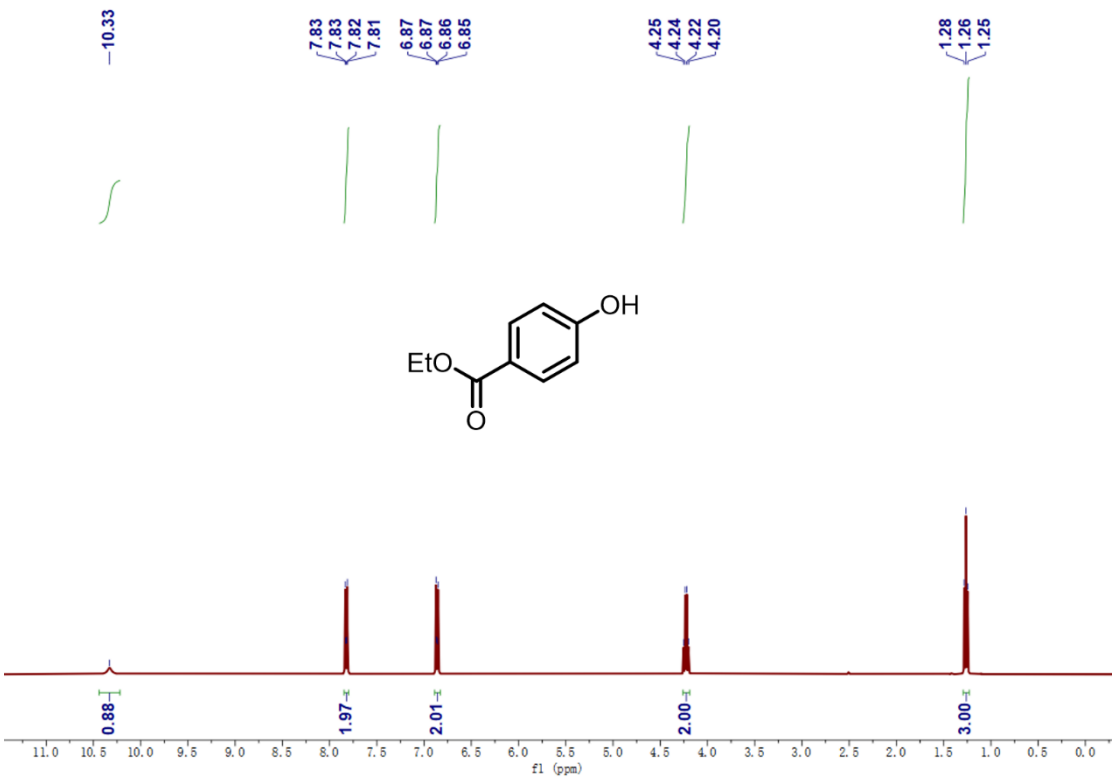

Fig. S53 ^{1}H NMR spectra of **4m** in DMSO-*d*6.

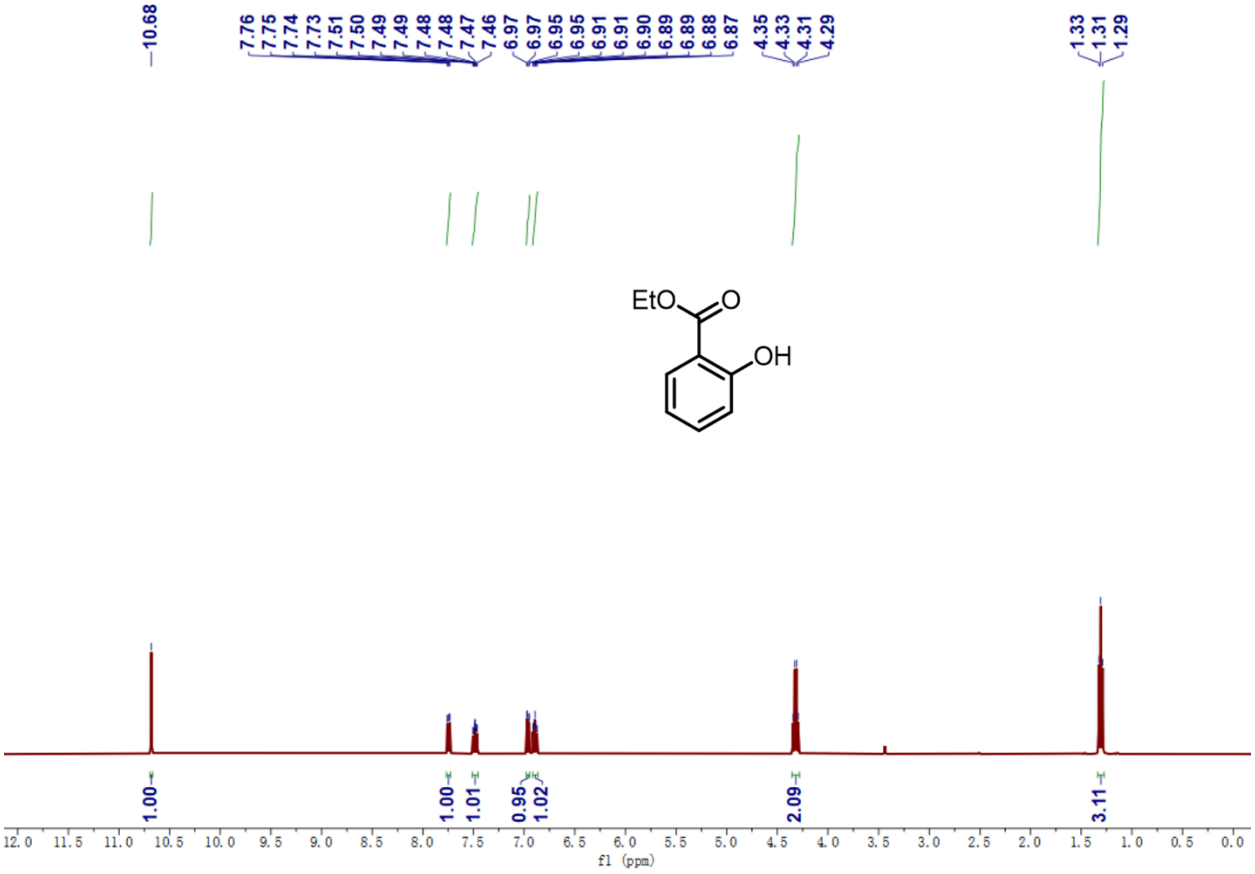

Fig. S54 ^{1}H NMR spectra of **4n** in DMSO-d_6.

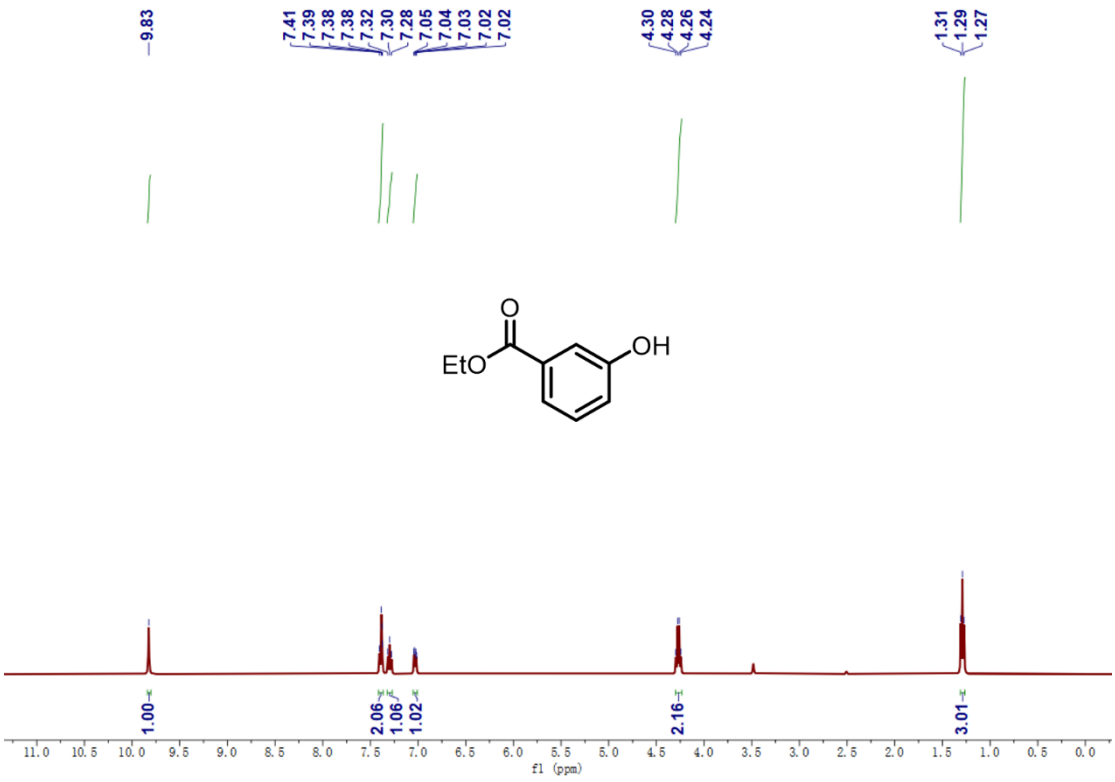

Fig. S55 ^{1}H NMR spectra of **4o** in DMSO-d_6.

^{1}H NMR data of 2a-2l

2a. (Methylsulfinyl)benzenee

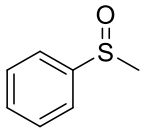

^{1}H NMR (400 MHz, $CDCl_3$) δ 7.66 (dd, *J* = 8.0, 1.6 Hz, 2H), 7.53 (d, *J* = 7.5 Hz, 3H), 2.74 (s, 3H).

2b. 1-Methyl-4-(methylsulfinyl)benzene

^{1}H NMR (400 MHz, $CDCl_3$) δ 8.37 (d, *J* = 8.8 Hz, 2H), 7.82 (d, *J* = 8.8 Hz, 2H), 2.78 (s, 3H).

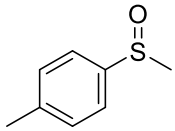

2c. 1-Methoxy-4-(methylsulfinyl)benzenec

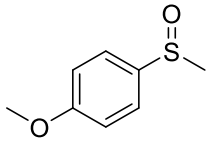

^{1}H NMR (400 MHz, $CDCl_3$) δ 7.58 (d, *J* = 8.8 Hz, 2H), 7.02 (d, *J* = 8.8 Hz, 2H), 3.84 (s, 3H), 2.69 (s, 3H).

2d. 1-Methoxy-2-(methylsulphinvl)benzene

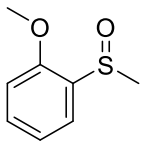

^{1}H NMR (400 MHz, $CDCl_3$) δ 7.79 (dd, *J* = 7.7, 1.7 Hz, 1H), 7.43 (ddd, *J* = 8.2, 7.4, 1.7 Hz, 1H), 7.17 (td, *J* = 7.6, 1.0 Hz, 1H), 6.90 (dd, *J* = 8.2, 0.9 Hz, 1H), 3.87 (s, 3H), 2.75 (s, 3H).

2e. 1-Ethynyl-4-(methylsulfinyl)benzene

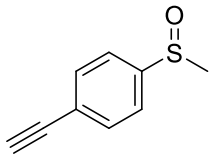

^{1}H NMR (400 MHz, $CDCl_3$) δ 7.83-7.76 (m, 2H), 7.75-7.69 (m, 2H), 2.72 (s, 3H).

2f. 1-Fluoro-4-(methylsulfinyl)benzenee

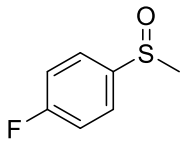

^{1}H NMR (400 MHz, $CDCl_3$) δ 7.68-7.56 (m, 2H), 7.23-7.14 (m, 2H), 2.68 (s, 3H).

2g. 1-Chloro-4-(methylsulfinyl)benzene

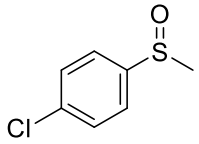

^{1}H NMR (400 MHz, $CDCl_3$) δ 7.55-7.49 (m, 2H), 7.46-7.40 (m, 2H), 2.65 (s, 3H).

2h. 1-Chloro-2-(methylsulphinyl)benzene

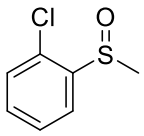

^{1}H NMR (400 MHz, $CDCl_3$) δ 7.87 (dd, *J* = 7.8, 1.7 Hz, 1H), 7.46 (td, *J* = 7.5, 1.3 Hz, 1H), 7.41-7.28 (m, 2H), 2.75 (s, 3H).

2i. 1-Bromo-4-(methylsulfinyl)benzene

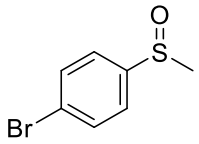

^{1}H NMR (400 MHz, $CDCl_3$) δ 7.61-7.54 (m, 2H), 7.48-7.40 (m, 2H), 2.63 (s, 3H).

2j. 1-Bromo-2-(methylsulfinyl)benzene

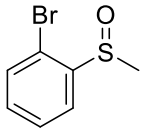

^{1}H NMR (400 MHz, $CDCl_3$) δ 7.90 (dd, *J* = 7.8, 1.6 Hz, 1H), 7.57-7.50 (m, 2H), 7.34 (ddd, *J* = 8.0, 7.3, 1.7 Hz, 1H), 2.78 (s, 3H).

2k. 1-Methanesulfinyl-4-nitrobenzene

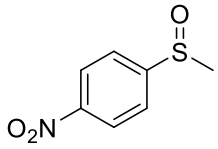

^{1}H NMR (400 MHz, $CDCl_3$) δ 7.52 (d, *J* = 8.2 Hz, 2H), 7.34-7.29 (m, 2H), 2.69 (s, 3H), 2.40 (s, 3H).

2l. 4-(Methylsulfinyl)benzaldehyde

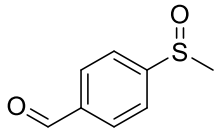

^{1}H NMR (400 MHz, $CDCl_3$) δ 8.37 (d, *J* = 8.8 Hz, 2H), 7.82 (d, *J* = 8.8 Hz, 2H), 2.78 (s, 3H).

^{1}H NMR data of 4a-4o

4a. 4-Hydroxypyridine

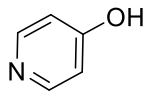

^{1}H NMR (400 MHz, DMSO-d_6) δ 7.27-7.21 (m, 2H), 6.93 (tt, J = 7.4, 1.1 Hz, 1H), 6.89-6.77 (m, 2H), 5.23 (s, 1H).

4b. Phenylboronic acid

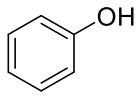

^{1}H NMR (400 MHz, $CDCl_3$) δ 7.27-7.22 (m, 2H), 6.95-6.90 (m, 1H), 6.85-6.81 (m, 2H), 5.23 (s, 1H).

4c. 4-Methylphenol

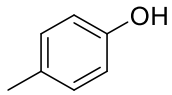

^{1}H NMR (400 MHz, DMSO-d_6) δ 9.12 (s, 1H), 7.03-6.87 (m, 2H), 6.64 (d, J = 8.4 Hz, 2H), 2.17 (s, 3H).

4d. 4-Fluorophenol

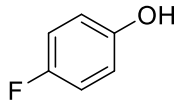

^{1}H NMR (400 MHz, $CDCl_3$) δ 6.98-6.88 (m, 2H), 6.82-6.73 (m, 2H), 5.28 (s, 1H).

4e. 4-Chlorophenol

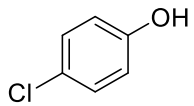

^{1}H NMR (400 MHz, $CDCl_3$) δ 7.55-7.49 (m, 2H), 7.46-7.40 (m, 2H), 2.65 (s, 3H).

4f. 4-Bromophenol

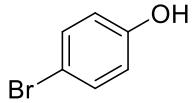

^{1}H NMR (400 MHz, $CDCl_3$) δ 7.37-7.28 (m, 2H), 6.76-6.66 (m, 2H), 5.25 (s, 1H).

4g. 4-Nitrophenol

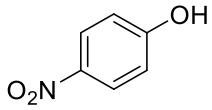

^{1}H NMR (400 MHz, DMSO-d_6) δ 11.08 (s, 1H), 8.09 (d, *J* = 9.2 Hz, 2H), 6.91 (d, *J* = 9.2 Hz, 2H).

4h. 4-Hydroxybenzaldehyde

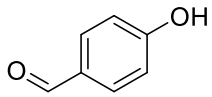

^{1}H NMR (400 MHz, $CDCl_3$) δ 9.79 (s, 1H), 7.76 (d, *J* = 8.6 Hz, 2H), 6.93 (d, *J* = 8.6 Hz, 2H).

4i. 3-Hydroxybenzaldehyde

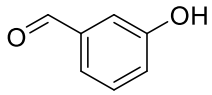

^{1}H NMR (400 MHz, $CDCl_3$) δ 9.95 (s, 1H), 7.47-7.39 (m, 3H), 7.16 (ddd, *J* = 7.1, 2.6, 1.9 Hz, 1H).

4j. 2-Hydroxybenzonitrile

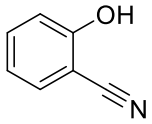

^{1}H NMR (400 MHz, DMSO-d_6) δ 11.08 (s, 1H), 7.58 (dd, *J* = 7.8, 1.7 Hz, 1H), 7.48 (ddd, *J* = 8.9, 7.4, 1.7 Hz, 1H), 7.00 (dd, *J* = 8.5, 1.0 Hz, 1H), 6.91 (td, *J* = 7.5, 1.0 Hz, 1H).

4k. 3-Hydroxybenzonitrile

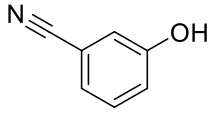

^{1}H NMR (400 MHz, $CDCl_3$) δ 7.35 (t, *J* = 7.9 Hz, 1H), 7.23 (dt, *J* = 7.7, 1.3 Hz, 1H), 7.19-7.12 (m, 2H).

4l. 5-Hydroxypyrimidine

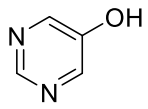

^{1}H NMR (400 MHz, DMSO-d_6) δ 10.52 (s, 1H), 8.66 (s, 1H), 8.33 (s, 2H).

4m. Ethyl 4-hydroxybenzoate

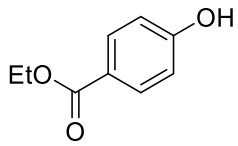

^{1}H NMR (400 MHz, DMSO-d_6) δ 10.33 (s, 1H), 7.85-7.80 (m, 2H), 6.89-6.83 (m, 2H), 4.23 (q, J = 7.1 Hz, 2H), 1.26 (t, J = 7.1 Hz, 3H).

4n. Ethyl 2-hydroxybenzoate

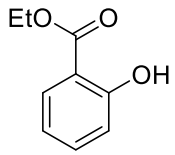

^{1}H NMR (400 MHz, DMSO-d_6) δ 10.68 (s, 1H), 7.75 (dd, J = 8.0, 1.8 Hz, 1H), 7.48 (ddd, J = 8.4, 7.2, 1.8 Hz, 1H), 6.96 (dd, J = 8.4, 1.2 Hz, 1H), 6.89 (ddd, J = 8.2, 7.2, 1.2 Hz, 1H), 4.32 (q, J = 7.1 Hz, 2H), 1.31 (t, J = 7.2 Hz, 3H).

4o. Ethyl 3-hydroxybenzoate

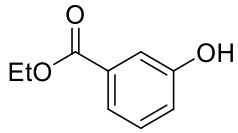

^{1}H NMR (400 MHz, DMSO-d_6) δ 9.83 (s, 1H), 7.41-7.37 (m, 2H), 7.30 (t, J = 7.8 Hz, 1H), 7.03 (dd, J = 9.0, 2.5 Hz, 1H), 4.27 (q, J = 7.1 Hz, 2H), 1.29 (t, J = 7.1 Hz, 3H).

References:

S1. V.-N. Nguyen, S. Qi, S. Kim, N. Kwon, G. Kim, Y. Yim, S. Park, and J. Yoon, *J. Am. Chem. Soc.*, 2019, **141**, 16243−16248.

S2. G. Linden, L. Zhang, F. Pieck, U. Linne, D. Kosenkov, R. Tonner, and O. Vázquez, *Angew. Chem. Int. Ed.*, 2019, **58**, 12868 –12873.

S3. M. K. Kuimova, H. A. Collins, M. Balaz, E. Dahlstedt, J. A. Levitt, N. Sergent, K. Suhling, M. Drobizhev, N. S. Makarov, A. Rebane, H. L. Anderson and D. Phillips, *Org. Biomol. Chem.*, 2009, **7**, 889–896.

S4. Y. Hao, B. M. Liu, T. F. Bennett, C. G. Monsour, M. Selke, Y. Liu, *J. Phys. Chem. C*, 2021, **125**, 7392−7400.

S5. X. Kan, J.-C. Wang, Z. Chen, J.-Q. Du, J.-L. Kan, W.-Y. Li, and Y.-B. Dong, *J. Am. Chem. Soc.*, 2022, **144**, 6681−6686.

S6. R. Zhang, G. Feng, C.-J. Zhang, X. Cai, X. Cheng, and B. Liu, *Anal. Chem.*, 2016, **88**, 4841−4848.

S7. Y. Gao, X. Wang, X. He, Z. He, X. Yang, S. Tian, F. Meng, D. Ding, L. Luo, and B. Z. Tang, *Adv. Funct. Mater.*, 2019, **29**, 1902673

S8. X. Dong, X. Dai, G. Li, Y.-M. Zhang, X. Xu, and Y. Liu, *Adv. Sci.*, 2022, 2201962.

S9. M. P. Donzello, E. Viola, M. Giustini, C. Ercolani and F. Monacelli, *Dalton Trans.*, 2012, **41**, 6112-6121.

S10. E. A. Dupouy, D. Lazzeri and E. N. Durantini, *Photochem. Photobiol. Sci.*, 2004, **3**, 992-998.

S11. G. Schnurpfeil, A. K. Sobbi, W. Spiller, H. Kleisch and D. Wohrle, *J. Porphyrins Phthalocyanines*, 1997, 01, 159-167.

S12. E. H. Mørkved, T. Andreassen, V. Novakova and P. Zimcik, *Dyes Pigm.*, 2009, **82**, 276-285.

S13. U. Michelsen, H. Kliesch, G. Schnurpfeil, A. K. Sobbi and D. Wohrle, *Photochem. Photobiol.*, 1996, **64**, 694-701.

S14. T. C. Tempesti, M. G. Alvarez, E. N. Durantini, *Dyes Pigm.*,2011, **91**, 6-12.

S15. M. Machacek, J. Kollár, M. Miletin, R. Kučera, P. Kubát, T. Simunek, V. Novakova and P. Zimcik, *RSC Adv.*, 2016, **6**, 10064-10077.

S16. P. Zimcik, M. Miletin, H. Radilova, V. Novakova, K. Kopecky, J. Svec, E. Rudolf, *Photochem. Photobiol.*, 2010, **86**, 168-175.

S17. G. De Mori, Z. Fu, E. Viola, X. H. Cai, C. Ercolani, M. P. Donzello and K. M. Kadish, *Inorg. Chem.*, 2011, **50**, 8225-8237.

S18. B. Ghazal, M. Machacek, M. A. Shalaby, V. Novakova, P. Zimcik and S. Makhseed, *J. Med. Chem.*,2017, **60**, 6060-6076.

S19. V. Novakova, R. Z. Uslu Kobak, R. Kucera, K. Kopecky, M. Miletin, V. Krepsova, J. Ivincova and P. Zimcik, *Dalton Trans.*, 2012, **41**,10596-10604.

S20. S. Makhseed, A. Tuhl, J. Samuel, P. Zimcik, N. Al-Awadi and V. Novakova, *Dyes Pigm.*, 2012, **95**, 351-357.

S21. M. P. Donzello, D. Vittori, E. Viola, L. H. Zeng, Y. Cui, K. M. Kadish, L. Mannina and C. Ercolani, *J. Porphyrins Phthalocyanines*, 2015, **19**, 903-919.

S22. C. J. Song, J. M. Park, W. Yao, C. Y. Jung and J. Y. Jaung, *J. Porphyrins Phthalocyanines*, 2015, **19**, 967-972.

S23. T. C. Tempesti, J. C. Stockert and E. N. Durantini, *J. Phys. Chem. B*, 2008, **112**, 15701-15707.

S24. E. A. Dupouy, D. Lazzeri and E. N. Durantini, *Photochem. Photobiol. Sci.*, 2004, **3**, 992-998.

S25. M. B. Spesia, M. Rovera and E. N. Durantini, *Eur. J. Med. Chem.*, 2010, **45**, 2198-2205.

S26. C. A. Suchetti and E. N. Durantini, *Dyes Pigm.*, 2007, **74**, 630-635.

S27. M. Machacek, J. Demuth, P. Cermak, M. Vavreckova, L. Hruba, A. Jedlickova, P. Kubat, T. Simunek, V. Novakova and P. Zimcik, *J. Med. Chem.*, 2016, **59**, 9443-9456.

S28. H. Huang, X. Han, X. Li, S. Wang, P. K. Chu, Y. Zhang, *ACS Appl. Mater. Interfaces*, 2015, **7**, 482-492.

S29. L. Ye, J. Liua, Z. Jiang, T. Peng, L. Zan, *Appl. Catal. B Environ.*, 2013,**142-143**,1-7.

S30. Y. Li, W. Zhang, J. Niu, Y. Chen, *ACS Nano*, 2012, **6**, 5164-5173.